The chromatin remodeler p400 ATPase facilitates Rad51-mediated repair of DNA double-strand breaks

Céline Courilleau,[1,2] Catherine Chailleux,[1,2] Alain Jauneau,[3] Fanny Grimal,[4] Sébastien Briois,[1,2] Elisa Boutet-Robinet,[5,6] François Boudsocq,[7] Didier Trouche,[1,2] and Yvan Canitrot[1,2]

[1]Laboratoire de Biologie Cellulaire et Moléculaire du Contrôle de la Prolifération, UMR 5088, Université de Toulouse and [2]Centre National de la Recherche Scientifique, Université Paul Sabatier, 31062 Toulouse, France
[3]FR3450 Plateforme Microscopie imagerie, Pôle Biotechnologie Végétale, Centre National de la Recherche Scientifique, 31326 Castanet Tolosan, France
[4]Centre de Recherche en Cancérologie de Toulouse, UMR 1037, Institut National de la Santé et de la Recherche Médicale, Université de Toulouse, 31024 Toulouse, France
[5]Toxalim, Research Centre in Food Toxicology, UMR 1131, Institut National de la Recherche Agronomique and [6]Université de Toulouse, 31027 Toulouse, France
[7]Laboratoire de Biologie Moléculaire Eucaryote, UMR 5099, Centre National de la Recherche Scientifique, Université de Toulouse, 31062 Toulouse, France

DNA damage signaling and repair take place in a chromatin context. Consequently, chromatin-modifying enzymes, including adenosine triphosphate–dependent chromatin remodeling enzymes, play an important role in the management of DNA double-strand breaks (DSBs). Here, we show that the p400 ATPase is required for DNA repair by homologous recombination (HR). Indeed, although p400 is not required for DNA damage signaling, DNA DSB repair is defective in the absence of p400. We demonstrate that p400 is important for HR-dependent processes, such as recruitment of Rad51 to DSB (a key component of HR), homology-directed repair, and survival after DNA damage. Strikingly, p400 and Rad51 are present in the same complex and both favor chromatin remodeling around DSBs. Altogether, our data provide a direct molecular link between Rad51 and a chromatin remodeling enzyme involved in chromatin decompaction around DNA DSBs.

Introduction

The genome of eukaryotic cells is the target of intracellular or extracellular DNA damaging agents. To maintain genetic information, cells use well-defined DNA repair pathways (Hoeijmakers, 2001). DNA double-strand breaks (DSBs) are one of the more deleterious forms of DNA damage that are repaired by two main pathways: non-homologous end joining (NHEJ) and homologous recombination (HR). The genome is assembled into chromatin, a complex structure the repair machinery has to deal with to efficiently repair DNA damages. In response to DNA damage, chromatin undergoes remodeling and decompaction (Kruhlak et al., 2006; Ziv et al., 2006). In yeast, ATP-dependent chromatin remodeling enzymes that modify the local nucleosome concentration or the composition of chromatin by introducing histone variants (Clapier and Cairns, 2009) are implicated in the changes of chromatin structure in response to DNA damages (Kusch et al., 2004; Mizuguchi et al., 2004). These enzymes belong to the SWI/SNF superfamily and can be classified in four families (SWI/SNF, ISWI, CHD/Mi2, and INO80) defined by yeast proteins. In yeast, enzymes from the four families (Ino80, Swr1, RSC, and SWI/SNF) remodel nucleosomes around DSB to facilitate DNA repair and/or to regulate cell cycle (Downs et al., 2004; Morrison et al., 2004; van Attikum et al., 2004; Chai et al., 2005; Tsukuda et al., 2005; van Attikum et al., 2007; Oum et al., 2011). In human cells, the CHD4 and MTA2 subunits of CHD complexes are recruited in the vicinity of DSB and participate in the DNA damage response (Ahel et al., 2009; Gottschalk et al., 2009; Chou et al., 2010; Larsen et al., 2010; Smeenk et al., 2010). In addition, ACF1 and SNF2H, two members of the ISWI family, are involved in NHEJ and HR mechanisms (Lan et al., 2010). BRG1, a subunit of the SWI/SNF complex is recruited to DSB via H3 acetylation and stimulates the amplification of H2AX phosphorylation probably by facilitating accessibility to nucleosomes around DSB (Lee et al., 2010). Finally, among ATPases

D. Trouche and Y. Canitrot contributed equally to this paper.

Correspondence to Yvan Canitrot: canitrot@cict.fr

Abbreviations used in this paper: ChIP, chromatin immunoprecipitation; DSB, double-strand break; FRET, fluorescence resonance energy transfer; FLIM, fluorescence lifetime imaging microscopy; HDR, homology-directed repair; HR, homologous recombination; IR, ionizing radiation; MEF, mouse embryonic fibroblast; NHEJ, non-homologous end joining; OHTam, 4-hydroxy-tamoxifen.

The Rockefeller University Press $30.00
J. Cell Biol. Vol. 199 No. 7 1067–1081
www.jcb.org/cgi/doi/10.1083/jcb.201205059

of the INO80 family, p400 and INO80 are recruited at DSB and control histone ubiquitination or the 5′-3′ resection of DNA ends, respectively (Xu et al., 2010; Gospodinov et al., 2011). These studies showed the requirement of chromatin modification and remodeling to allow the appropriate response to DNA damage. However, the complexes studied in these works participate in DNA damage signaling or in early steps of DSB repair and their involvement in the later stages of these mechanisms is still poorly studied.

One of the enzymes promoting chromatin remodeling is the p400 ATPase, which belongs to the INO80 family (Fuchs et al., 2001; Ruhf et al., 2001). p400 is involved in the transcriptional control of specific genes through the incorporation of the histone variant H2AZ on promoters (Gévry et al., 2007). It belongs to a multimolecular complex containing the histone acetyl transferase Tip60 (Ikura et al., 2000). Interestingly, Tip60 is important for the DNA damage response by promoting ATM activation (Sun et al., 2005) and the subsequent H2AX phosphorylation (Ikura et al., 2007) and by acetylating histones to allow recruitment of DNA repair proteins (Murr et al., 2006). In addition, the p400 homologue in *Saccharomyces cerevisiae* SWR1 is recruited to DNA breaks and is important for DNA repair by NHEJ (van Attikum et al., 2007). Moreover, some links between SWR1 and HR have been described: when strand invasion is made defective because of the absence of homologous sequences, SWR1 functionally cooperates with Rad51, a key protein of HR, to target DNA breaks to the nuclear periphery (Kalocsay et al., 2009). In *Drosophila melanogaster* and yeast, p400 homologues are important to remove phosphorylated H2AX from chromatin after the completion of DNA repair (Kusch et al., 2004; Papamichos-Chronakis et al., 2006). Finally, a recent study found that human p400 is important for DNA damage signaling (Xu et al., 2010), but its precise role in human DSB repair remains unclear. In this study we examined the role of p400 in response to DNA damage in human cells by characterizing its influence on DNA damage signaling and DSB repair.

Results

p400 expression is important upon DNA damage induction

To characterize the role of human p400 in DNA repair, we examined the sensitivity of p400-depleted cells to DNA damaging agents inducing DNA DSBs (bleomycin and ionizing radiations [IR]). U2OS cells transfected with p400 siRNA (extensively validated in previous studies [Tyteca et al., 2006; Mattera et al., 2009, 2010]; see Fig. S1 for Western blots monitoring the effects of the various siRNAs) harbor increased sensitivity to these agents (Fig. 1 A). This sensitivity is comparable, albeit slightly lower, to that observed upon depletion of a known DNA damage response protein, ATM (Fig. 1 A). Thus, p400 expression influences the response and/or the repair of the DNA damages induced by these treatments, such as DSBs. We next analyzed the formation of γH2AX foci, a commonly used marker of DSB. In nonirradiated cells, p400 knockdown is sufficient to induce γH2AX foci (Fig. 1, B and C), reflecting DNA breaks induced by increased oxidative stress (Mattera et al., 2010). One hour after IR, most cells harbor strong γH2AX staining (Fig. 1, B and C) both in control and p400-depleted cells (although these latter ones exhibit brighter foci than control cells [Fig. S2 A]). At longer time points, the number of γH2AX-positive cells decreases in control cells, reflecting DNA repair. Strikingly, in p400-depleted cells, this decrease is slower. Western blot analysis of γH2AX also confirms that γH2AX levels are higher upon p400 knockdown (Fig. 1 D). Similar effects are observed in mouse embryonic fibroblasts (MEFs) generated from mice expressing truncated p400 protein (Ueda et al., 2007; Fig. S2 B), indicating that they are neither cell type specific, nor a particular property of transformed cells, nor a result of siRNA off-target effects. To test whether these results are because of an increased DNA damage signaling or to a defect in DNA repair, we monitored γH2AX foci formation in a more extensive time course experiment. Indeed, the number of foci roughly reflects the number of DNA breaks, and the kinetics of γH2AX foci numbers decrease is an indication of DNA repair (Rogakou et al., 1999). To achieve statistical significance, we used a high-capacity device allowing automatic measurement and analysis of fluorescence (Arrayscan) for individual cells. This allows a powerful statistical analysis and a comprehensive study of the effects of p400 siRNA in a kinetic fashion using two doses of irradiation (2 and 8 Gy). Note that the settings of the automatic analysis were not necessarily identical for the 2- and 8-Gy irradiation points because we used settings that give the maximal difference between nonirradiated and irradiated cells with respect to foci numbers. Thus, we cannot compare directly the number of foci between these two conditions. Whiskers graphs of the cell populations respective to the number of γH2AX foci are shown in Fig. 1 (E and F), as well as the p-value for the difference between the control and p400-depleted populations. We first found that the number of foci at early time points after irradiation is roughly similar or slightly increased depending on the experiments upon p400 depletion, indicating that the amount of DNA breaks is similar. Similar results were obtained when monitoring the number of DSB by neutral comet assays (Figs. 1 G and S3 B, compare the 0 point). When looking at later time points, we noticed that p400 depletion slows down the decrease in γH2AX foci numbers (Fig. 1, E and F). For example, at 8 Gy irradiation, the apparent decrease in foci number between 15 min and 6 h after irradiation is roughly of 3 foci per hour for control cells and ∼1.5 foci per hour for p400-depleted cells (Fig. 1 E). This result suggests a defect in DNA DSB repair in p400-depleted cells. Given that multiple DSBs can cluster in the same γH2AX focus (Neumaier et al., 2012), we also directly analyzed DSB disappearance by neutral comet assay. Using this assay, we found a defect in DSB repair in p400-depleted U2OS cells (Fig. 1 G) as well as in p400-deficient MEFs (Fig. S3B).

In addition, the total γH2AX fluorescence per cell in the same samples is higher in p400-depleted cells (Fig. 2 A) even at early time points (15 min). Similar results are observed by Western blot 1 h after irradiation (Fig. 1 D). Because the number of breaks per cell is similar at these time points (Fig. 1, E and G), it indicates that p400 limits the phosphorylation of

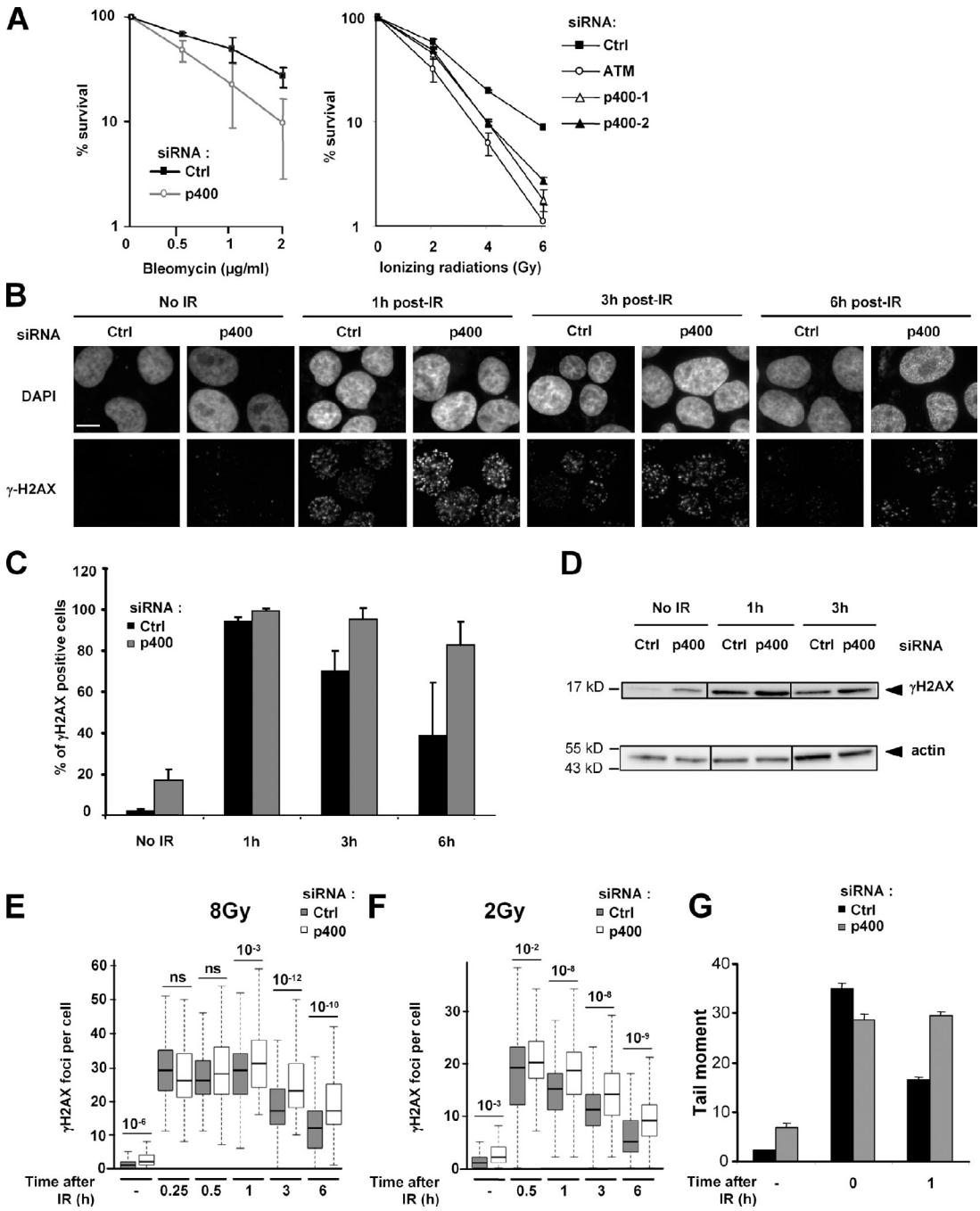

Figure 1. **p400 depletion sensitizes cells to DNA damage.** U2OS cells were transfected with siRNA against p400 or a control sequence (Ctrl) and subjected to the indicated treatment 48 h later. (A) 2 wk later, clonogenic efficiency was evaluated. Results are the mean ± SD from at least three independent experiments. (B) Cells were irradiated (8 Gy) or not and subjected to γH2AX immunofluorescence. Bar, 10 µm (C) Quantification of experiment in B. Results are the mean ± SD from five independent experiments. (D) cells were irradiated (8 Gy) or not and subjected to Western blot analysis for γH2AX. (E and F) Automatized analysis of γH2AX foci in cells irradiated at 8 (E) or 2 Gy (F). The number of foci per nucleus was counted for at least 200 nuclei. Whisker graphs representing the repartition of cells with respect to γH2AX foci numbers are shown with the median, the 50% median population (boxes), and the limits. The p-values for the difference between the two populations (Ctrl vs. p400 siRNA) are shown above each time point (NS, >5%). Similar results were obtained in two to four independent experiments. The 15-min point (F) was obviously aberrant and removed from the analysis. (G) Evaluation of DSB repair by neutral comet assay. U2OS cells transfected with siRNA were irradiated (20 Gy) 48 h later and subjected to comet assay. Tail moment was scored on 100 cells and results are expressed as the mean ± SEM.

H2AX. To test whether this is because of an inhibition of ATM activity, we checked ATM activation by Western blot using antibodies specific for phosphorylated ATM (S1981). We found that phosphorylated ATM levels are increased in p400-depleted cells 30 min after irradiation (Fig. 2 B, see the quantification at the top of the lanes). Thus, this result indicates that p400 limits ATM autophosphorylation and suggests that the increase in DNA damage signaling observed upon p400 knockdown is the result of a higher activation of ATM. Collectively, the results of Figs. 1 and 2 indicate that p400 plays a double role upon

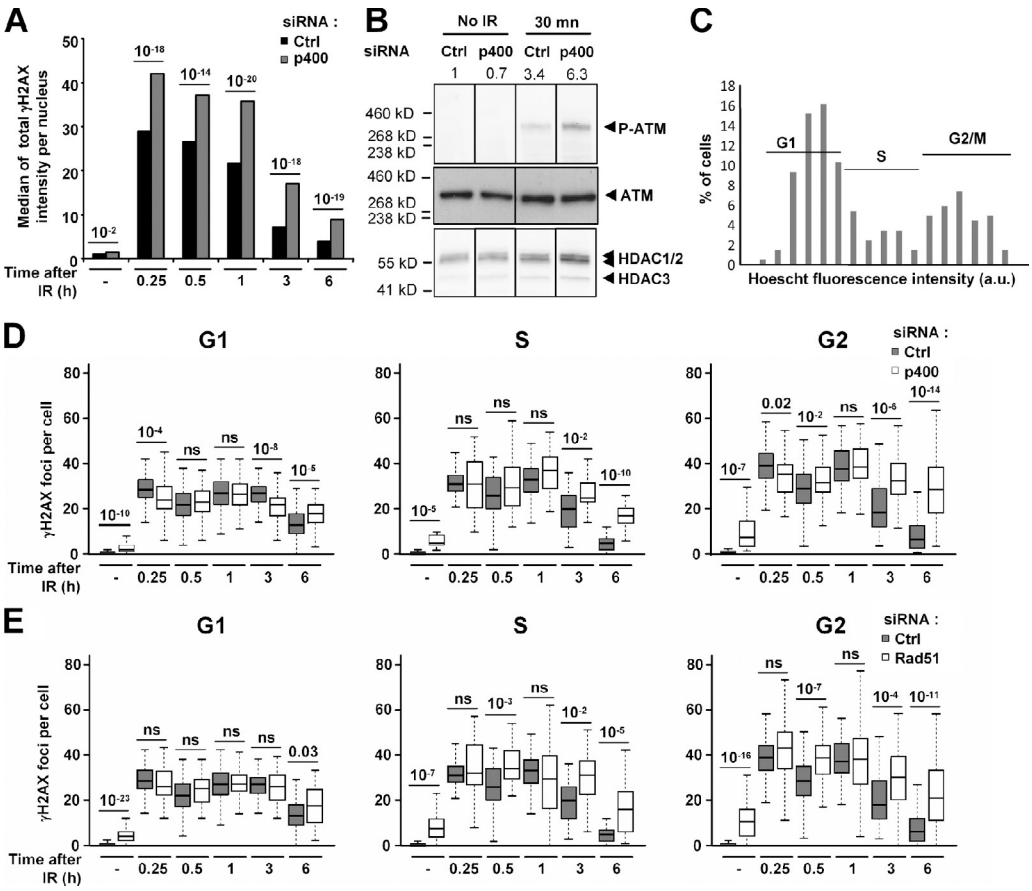

Figure 2. **p400 expression influences DNA damage signaling.** (A) Automatized analysis of total γH2AX fluorescence per nucleus (as in Fig. 1 E) of cells irradiated (8 Gy) or not. Median within the cell population is plotted and the p-values for the difference between the two populations (Ctrl vs. p400 siRNA) are shown above each time point. The data shown are from a single representative experiment (n = 200) out of three repeats. (B) U2OS cells transfected with p400 siRNA or a control sequence (Ctrl) were irradiated (8 Gy) or not and harvested 30 min later. Nuclear extracts were analyzed for total ATM, ATM phosphorylation on S1981, and HDAC1/2 expression by Western blot. Images were acquired using a charge-coupled device camera and levels of phosphorylated ATM were quantified using ImageJ software. (C) Example of cell cycle distribution obtained after Hoescht staining and Arrayscan quantification. n = 200 from a single experiment. The data shown are from a single representative experiment out of three repeats. (D) U2OS cells were transfected with p400 siRNA or control and irradiated or not (8 Gy). γH2AX foci number was analyzed as in Fig. 1 and whisker graphs representing the repartition of the cell population with respect to the number of foci for G1, S, and G2/M cells are shown. A representative experiment out of three is shown. (E) Same as in D, except that cells were transfected by control or Rad51 siRNA.

DNA DSB induction. First, it limits DNA damage signaling by controlling ATM activation. Second, it participates in DNA repair because DSB removal is slower upon p400 depletion.

p400 expression is important for HDR

We next investigated the role of p400 in DNA repair. To gain insights into the mechanism of repair that is affected by p400 depletion and given that HR, one of the main pathways responsible for DSB repair, is regulated in a cell cycle–dependent fashion, we analyzed γH2AX foci number in the various cell cycle phases. To do that, we sorted cells according to their DNA content. This was performed by measuring DNA content using Hoechst fluorescence intensity and plotting the number of cells relative to this fluorescence. As shown in Fig. 2 C, we obtain classical cell cycle profiles. We next analyzed the number of γH2AX foci for G1, S, and G2/M cells. As expected because the amount of DSBs is directly proportional to DNA amount, more foci are observed in G2/M cells compared with G1 (although not exactly twofold probably because of foci merging; Fig. 2 D). Interestingly, p400 depletion strongly increases the half-life of foci mainly for S and G2/M cells, but not, or very weakly, for G1 cells. Thus, the effects of p400 on DNA repair are more pronounced in S and G2, in agreement with a role in HR. Indeed, knocking down Rad51, a key protein of HR, using siRNA gives a similar phenotype (Fig. 2 E).

We next evaluated the effects of p400 depletion on HR efficiency. We used a U2OS reporter cell line containing an integrated substrate (Fig. S4 A) designed to measure the repair of a unique DSB induced by the I-SceI endonuclease (which does not cut the human genome) by homology-directed repair (HDR). The appearance of GFP-positive cells is dependent on HR between two inactive GFP copies (Puget et al., 2005). This cell line expresses the I-SceI enzyme fused to the ligand-binding domain of the estrogen receptor (ER-I-SceI). Sequence-specific DSB is induced by the nuclear relocalization of the enzyme after 4-hydroxy-tamoxifen (OHTam) treatment (Fig. S4 B). Upon OHTam addition to control cells, the number of GFP-positive cells increases (Fig. 3 A), reflecting HDR induced by the targeted DNA break. As expected, Rad51 depletion decreases the number of GFP-positive cells. Importantly, p400

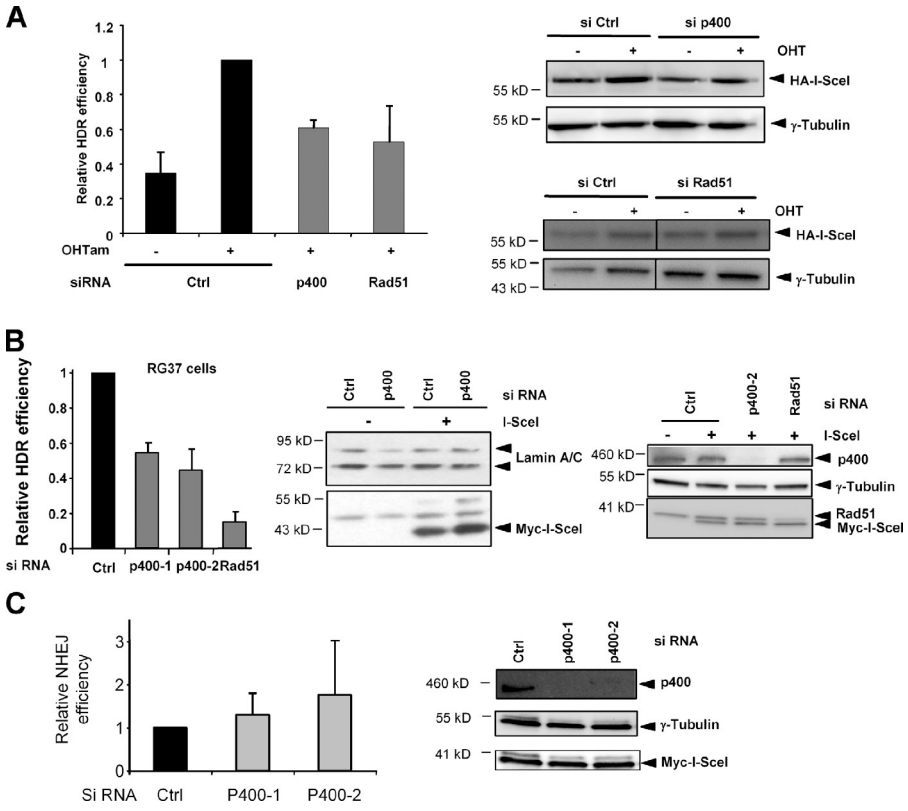

Figure 3. **p400 expression is important for HR.** (A) U2OS cells with an integrated HDR substrate and expressing ER-I-SceI were transfected with control, p400, or Rad51 siRNAs. 48 h after, cells were treated with OHTam, and 48 h later, GFP-positive cells were quantified by FACS. Results are the mean ± SD from three independent experiments. (right) Western blot monitoring HA-I-SceI expression. Note that HA-I-SceI–increased expression after OHTam addition is a result of stabilization after ligand binding. (B) RG37 cells with an integrated HDR substrate were transfected with control or two different p400 or Rad51 siRNA. 24 h after, the I-SceI expression plasmid was transfected, and HDR efficiency was monitored by FACS 48 h later. The mean ± SD from three independent experiments is plotted. (right) Western blots monitoring the indicated protein expressions are shown. (C) GCS5 cells with an integrated NHEJ substrate (Xie et al., 2009) were transfected with control or two different p400 siRNAs, and NHEJ efficiency was monitored by FACS 48 h later. The mean ± SD from four independent experiments is plotted. Statistical differences were examined using Student's *t* test (siCtrl vs. sip400-1 [P = 0.30] and siCtrl vs. sip400-2 [P = 0.31]). Western blots monitoring the expression of p400 and myc-I-SceI are shown.

depletion induces a similar decrease, indicating a defect in the repair of DSB by HDR. This is unlikely to be caused by inefficient cutting of the I-SceI site because p400 depletion does not affect I-SceI expression (Fig. 3 A). Thus, in U2OS cells, p400 depletion decreases the efficiency of HDR. However, previous work showed that the loss of p400 induces the expression of p21 in a p53-dependent manner and consequent accumulation of U2OS cells in G1 (Tyteca et al., 2006). This phenomenon could decrease HR activity, which is predominantly effective in S/G2. To check whether the decrease in HDR efficiency upon p400 depletion in U2OS cells is a consequence of G1 accumulation, we used a human cell line (RG37) that possesses an integrated substrate of HDR (Dumay et al., 2006) and in which the p53 pathway is largely inactivated by the SV40 T antigen (Meyn, 1993). As expected, in this assay, depletion of Rad51 decreases the number of GFP-positive cells (Fig. 3 B). p400 depletion using two different siRNAs decreases HDR efficiency, as in U2OS cells (Fig. 3 B), without inducing major changes in cell cycle distribution (Fig. S1 F), as expected. In addition, p400 depletion does not affect I-SceI cleavage efficiency, that we could measure in this experimental setting (Fig. S4 F). Because DSB could also be repaired by NHEJ we tested the effect of p400 depletion in cells with the same background than RG37. These cells stably express a NHEJ GFP reporter composed of a wild-type copy of the GFP gene in which translation is suppressed by an upstream, out of frame translation start site. Tandem DSBs introduced by I-SceI can release the out of frame translation start site and religation of the DNA ends allows translation of GFP in the correct frame (Xie et al., 2009). Using this cell line we find that p400 depletion does not induce significant changes in NHEJ activity (Fig. 3 C). Collectively, Fig. 3 results suggest that p400 expression is important for maximal HR efficiency.

p400 depletion does not affect DSB signaling in U2OS cells

DNA damage signaling leads to histone ubiquitination, which in turn facilitates recruitment of proteins involved in HR, such as BRCA1 and Rad51 (Luijsterburg and van Attikum, 2012). We thus transfected U2OS cells with p400 siRNA and examined ubiquitin-conjugated proteins after IR exposure using the FK2 antibody (Mailand et al., 2007). Ubiquitin foci are unchanged or slightly more abundant in p400-depleted cells regardless of the time and the dose of IR (Fig. 4, A and B). Moreover, the efficiency of foci formation of another DNA damage signaling protein, 53BP1, is not impaired upon p400 depletion (Fig. S2 C). These data are in contrast with a recent finding that 53BP1 and ubiquitin foci are decreased after overexpression of an inactive form of p400 (Xu et al., 2010). Because Xu et al. (2010) used a lower dose of IR and assayed foci formation at a shorter time, we performed a comprehensive analysis of 53BP1 and ubiquitin foci formation in a dose- and time-dependent fashion using the Arrayscan. In Fig. 4 C, we plotted the median within the cell population of the total amount of fluorescence within FK2 foci (which represent the total amount of ubiquitinated proteins present in signaling foci). We confirmed that no defect in both FK2 (Fig. 4 C) or 53BP1 (Fig. 4 F) foci formation is observable upon p400 depletion in U2OS submitted to 8 Gy at any time tested (the slight decrease for FK2 at the 15-min

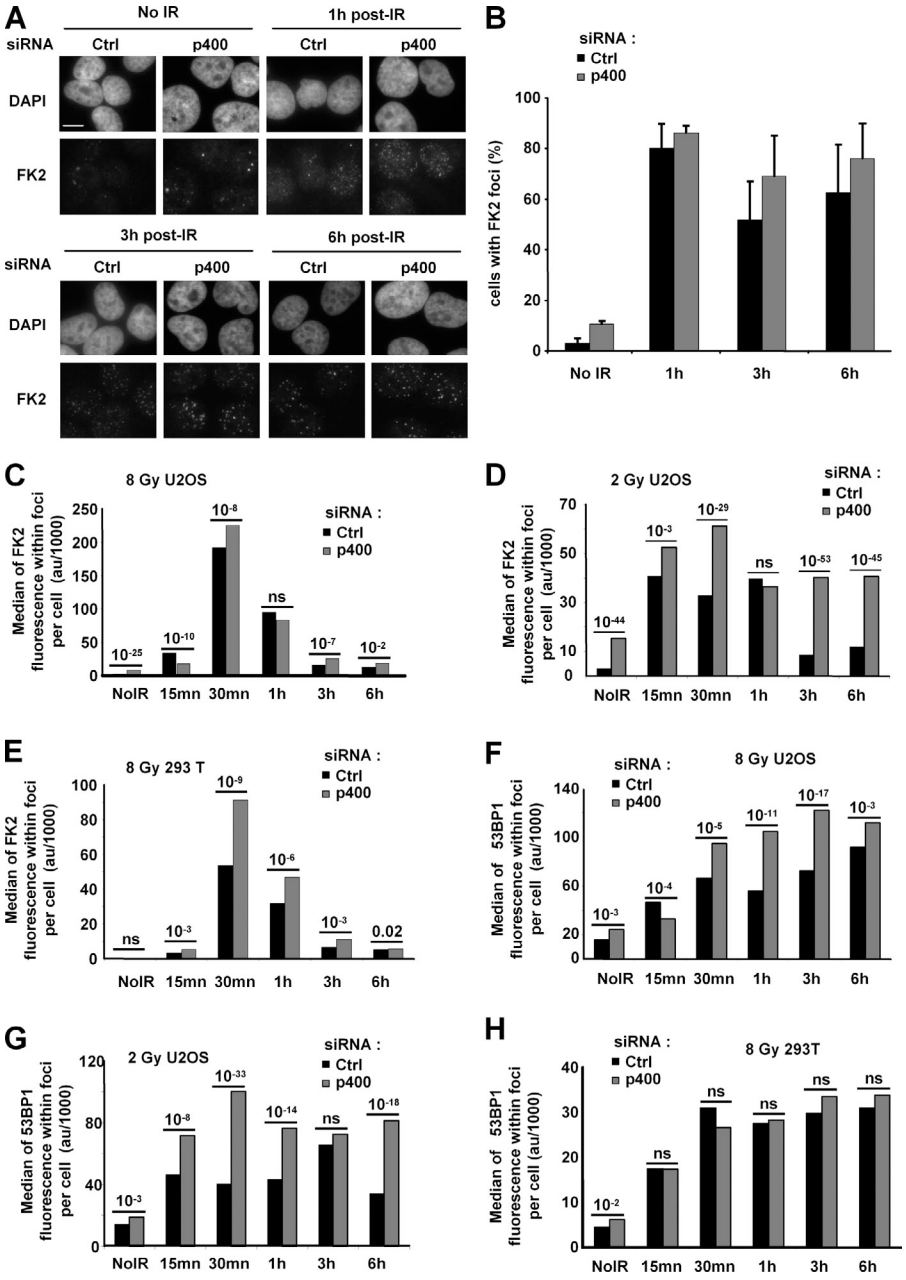

Figure 4. **DNA damage signaling is not affected by p400 knockdown.** (A and B) U2OS cells transfected with control or p400 siRNA were irradiated (8 Gy) or not 48 h later and subjected to FK2 immunofluorescence. Representative images (A) and quantifications are shown (B). Bar, 10 µm. Results are the mean ± SD from three independent experiments. (C and F) Automatized analysis of ubiquitin (FK2; C) or 53BP1 (F) foci in U2OS cells exposed to 8 Gy. Note that in other experiments the decrease was less pronounced after the 30-min peak of FK2 foci. (D and G) Automatized analysis of ubiquitin (FK2; D) or 53BP1 (G) foci in U2OS cells exposed to 2 Gy. (E and H) Automatized analysis of ubiquitin (FK2; E) or 53BP1 (H) foci in 293T cells exposed to 8 Gy. For C–H, the data shown are from a single representative experiment (n = 200) out of three repeats.

time point is not observed in other experiments nor using a lower dose of IR). We obtained similar results after 2-Gy exposure in U2OS cells (Fig. 4, D and G), and after 8 Gy in 293T cells (Fig. 4, E and H), which are the cells used in Xu et al. (2010). Finally, because Xu et al. (2010) used a dominant-negative mutant strategy, we transfected 293T cells with wild-type or ATPase-inactive p400 (containing the same inactivating mutation than in Xu et al. [2010]) and irradiated the cells (2 Gy). In contrast to that study, we did not observe any major difference with respect to ubiquitin foci or 53BP1 foci formation at 30 min and 1 h after irradiation (which are the time points examined by Xu et al. [2010]) upon expression of wild-type p400 or ATPase-inactive p400 mutant (Fig. S2, E–G). We conclude from Fig. 4 experiments that p400 depletion does not impair DNA damage signaling around DNA breaks.

p400 facilitates Rad51 recruitment to DNA breaks

We next analyzed the various steps of HR to characterize the molecular point in which p400 participates. HR begins by DNA resection, leading to the formation of single-strand DNA, which is covered by the RPA protein. To test whether the generation of single-strand DNA and RPA loading is affected by p400 depletion, we performed phospho-RPA immunofluorescence in U2OS cells. p400-depleted cells present slightly more phospho-RPA foci after IR than control cells (Fig. 5, A and B). This result was confirmed using the Arrayscan analysis (Fig. 5 C) as well as by Western blotting (unpublished data). Thus, p400 depletion does not decrease RPA phosphorylation, suggesting that the formation of single-strand DNA and RPA loading are normal. The next step in HR is the recruitment to the single-strand DNA of Rad51, which allows strand invasion

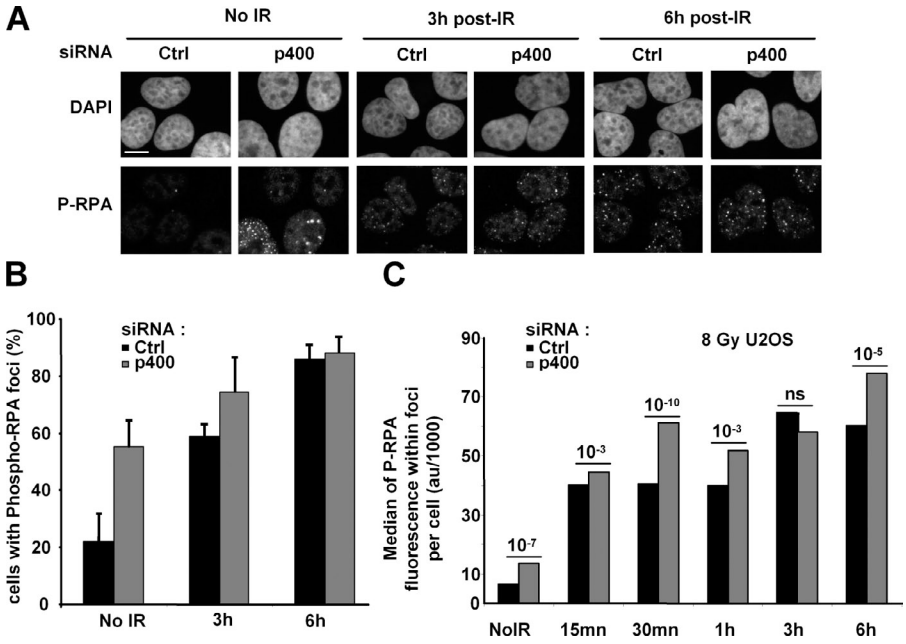

Figure 5. **RPA phosphorylation is not altered by p400 knockdown.** U2OS cells transfected with control or p400 siRNA were irradiated (8 Gy) or not 48 h later and subjected to phospho-RPA immunofluorescence after the indicated time. Representative images (A) and quantifications are shown (B). Bar, 10 µm. Results are the mean ± SD from three independent experiments. (C) Automatized analysis of phospho-RPA foci in U2OS cells treated as in A. Median within the cell population is plotted and the p-values for the difference between the two populations (Ctrl vs. p400 siRNA) are shown above each time point. The data shown are from a single representative experiment (n = 200) out of three repeats.

and promotes homologous pairing (Baumann et al., 1996). Functional HR involving Rad51 generates foci at the repair site that can be visualized by immunofluorescence (Haaf et al., 1995). We found that the Rad51 foci increase between 1 and 3 h after IR, depending on the experiment (Fig. 6). Strikingly, this increase, although still observable 6 h after IR, is largely delayed in cells transfected by the p400 siRNAs, as observed by manual counting (Fig. 6, A and B) or by automatic analysis using the Arrayscan device after 8 and 2 Gy, respectively (Fig. 6, C and D). This result suggests that the absence of p400 decreases the recruitment of Rad51 and accessory proteins to DSB. To test this possibility, we analyzed Rad51 recruitment at DSBs by chromatin immunoprecipitation (ChIP). We used a U2OS cell line in which AsiSI-mediated DSBs are induced by OHTam treatment (Iacovoni et al., 2010). ChIP assays revealed that Rad51 protein is present in control cells around DSB (Fig. 6 E, gray bars), and not on uncut chromatin. Strikingly, in p400-depleted cells, Rad51 recruitment to DSB is decreased (Fig. 6 E). This effect is not caused by a defect in enzyme accessibility because cleavage efficiency is slightly higher in p400-depleted cells (Fig. S4 C). Thus, p400 expression is required for Rad51 recruitment to chromatin. Similar results were obtained when analyzing the formation of the Rad51-associated protein BRCA1 foci by manual counting (Fig. 6, F and G) or by Arrayscan analysis after 8 and 2 Gy of IR (Fig. 6, H and I). Moreover, this effect on BRCA1 foci formation is also observed in 293T cells submitted to 8 Gy (Fig. 6 J; we did not manage to perform usable Rad51 immunofluorescence in 293T cells). These results indicate that p400 depletion delays the formation of Rad51 and BRCA1 foci.

The effect of p400 depletion on HR is not caused by cell cycle changes

Upon DSBs induction, Rad51 foci form in S and G2 cells but not in G1 cells. To check whether the decrease of Rad51 foci formation upon p400 depletion is not a consequence of G1 accumulation, we cotransfected U2OS cells with siRNA against p400 and p21 to reverse the p400-induced G1 arrest (Tyteca et al., 2006). Cells transfected with both p400 and p21 siRNAs are still defective in Rad51 foci formation in response to IR, although the G1 arrest is largely abolished (Fig. 7 A; and see Fig. S1, A and E, for p21 expression and cell cycle distribution). Finally, to rule out definitively any effects caused by changes in cell cycle distribution, we sorted cells according to cell cycle as described in Fig. 2 and we analyzed the formation of Rad51 foci. As expected, because the HR process is inhibited in G1, nearly no Rad51 foci are observed in G1 (Fig. 7 B). p400 depletion decreases the number of Rad51 foci for both S and G2/M cells (Fig. 7 B), demonstrating that the effect of p400 depletion can be observed independently of changes in cell cycle distribution. Moreover, it indicates that, although DNA damage signaling and HR does not rely exactly on the same mechanisms in S and G2 phase, p400 expression is important for Rad51 foci formation in both cell cycle phases.

p400 interacts with Rad51

Results from the aforementioned experiments indicate that p400 participates in Rad51-dependent steps. We thus examined whether p400 could directly affect Rad51 properties by physically interacting with it. We observed coimmunoprecipitation between endogenous Rad51 and p400 using three different antibodies against p400 (Fig. 8 A) in RG37 cells, a cell line with high level of p400 expression, indicating that Rad51 and p400 are present within the same multimolecular complex. Reciprocally, endogenous p400 is coimmunoprecipitated with Rad51 from HeLa nuclear extracts (Fig. 8 B). Moreover, p400 and Rad51 still coimmunoprecipitate in the presence of ethidium bromide, ruling out any artifacts as a result of the presence of DNA bridging the two proteins (unpublished data). When calculated relative to the input, the amount of interacting protein is very low, suggesting that

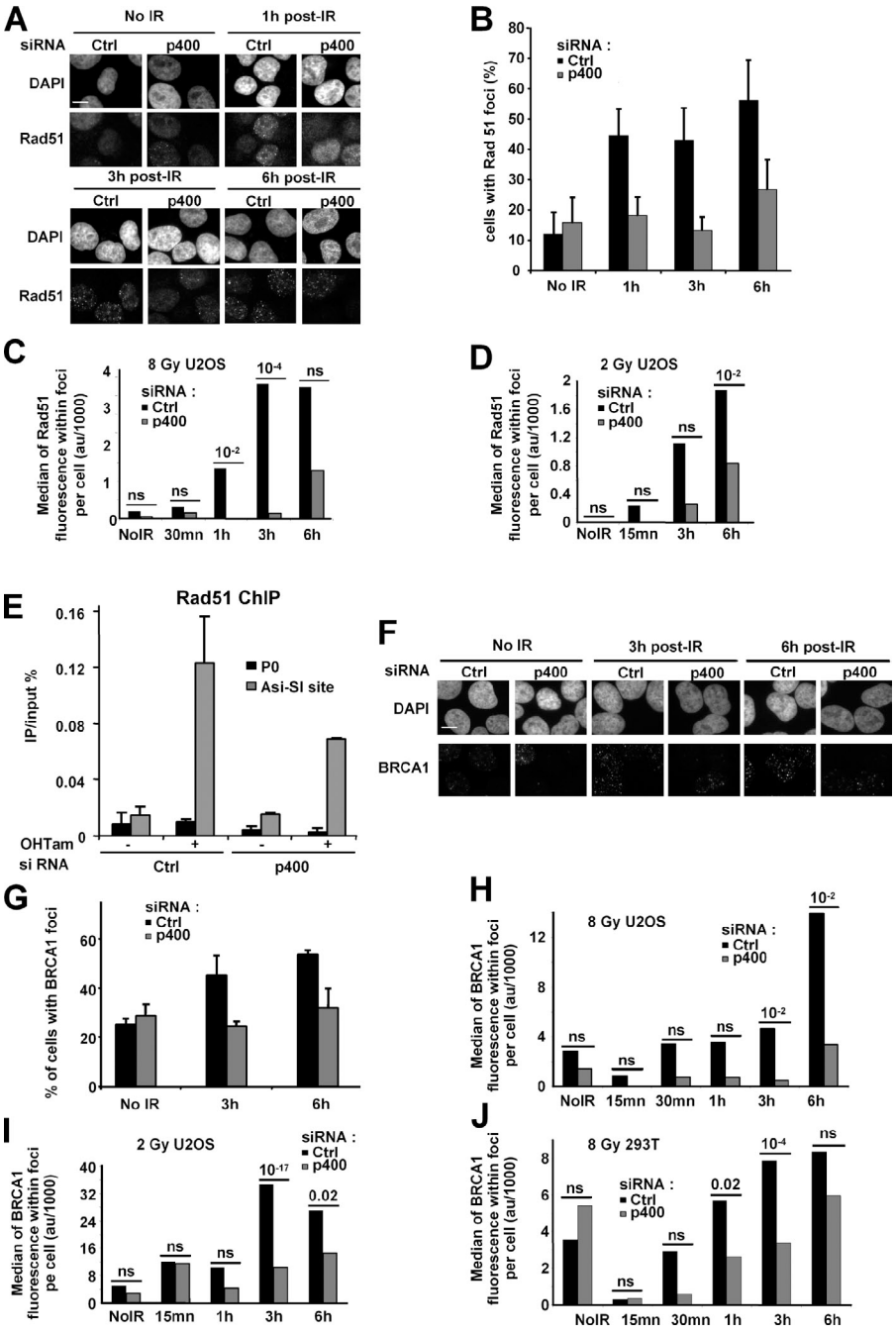

Figure 6. **p400 controls Rad51 foci formation.** (A and B) U2OS cells transfected with control or p400 siRNA were irradiated (8 Gy) or not 48 h later and subjected to Rad51 immunofluorescence. Bar, 10 µm. Representative images and quantifications are shown. Results are the mean ± SD from four independent experiments. (C) Automatized analysis of Rad51 foci in U2OS cells exposed to 8 Gy. Note that the Arrayscan failed to analyze the 15-min sample. (D) Automatized analysis of Rad51 foci in U2OS cells exposed to 2 Gy. Note that the Arrayscan failed to analyze the 30-min and 1-h samples. (E) 48 h after transfection with control or p400 siRNA, U2OS-ER-AsiSI cells were treated or not with OHTam (4 h) and subjected to ChIP experiment using anti-Rad51 antibodies. The amount of a sequence located 200 bp from a cleaved Asi-SI site and of a control sequence (P0) were quantified by qPCR. The mean ± SD from three independent experiments is shown. (F and G) U2OS cells transfected with control or p400 siRNA were irradiated (8 Gy) or not 48 h later and subjected to BRCA1 immunofluorescence. Representative images and quantifications are shown. Bar, 10 µm. Results are the mean ± SD from four independent experiments. Automatized analysis of BRCA1 foci in U2OS cells exposed to 8 Gy (H) and 2 Gy (I), respectively. The 30-min point that was obviously aberrant and not reproducible is not shown. (J) Automatized analysis of BRCA1 foci in 293T cells exposed to 8 Gy. For C, D, and H–J, the median within the cell population is plotted and the p-values for the difference between the two populations (Ctrl vs. p400 siRNA) are shown above each time point. The data shown are from a single representative (n = 200) experiment out of three repeats.

only a low proportion of both Rad51 and p400 are present in the same complex or that their interaction is dynamic. To gain insight into the dynamics of the p400–Rad51 interaction and to test their spatial proximity in cells, we performed fluorescence resonance energy transfer (FRET)/fluorescence lifetime imaging microscopy (FLIM) experiments. Transfection of RG37 cells with GFP-Rad51, which acts as the donor fluorophore and mcherry-p400 as the acceptor fluorophore, allows FRET-based approaches in fixed RG37 cells. If the two proteins are in very close proximity, the fluorescence half-life of GFP is shortened in proportion with the intensity of the energy transfer to the mcherry fluorophore. The lifetime of GFP is 2.60 ± 0.03 ns for cells transfected with GFP-Rad51 only and is not changed by the cotransfection of the empty mcherry vector (2.67 ± 0.05) (Figs. 8 C and S5). When cotransfected with mcherry-p400, this value is reduced to 2.19 ± 0.02 (representing 15.6% variation in fluorescence lifetime). Similar fluorescence transfer is observed between Tip60 and p400 (Fig. S5), two directly interacting proteins (Park et al., 2010), whereas no transfer is detected between 53BP1-GFP and p400-cherry (unpublished data), underlining the specificity of our observations. Thus, Rad51 and p400 are very close in cells. Moreover, given that FRET/FLIM is usually considered to monitor direct interactions (Llères et al., 2010; Nievergall et al., 2010), this result suggests that p400 and Rad51 directly interact in cells. We next investigated

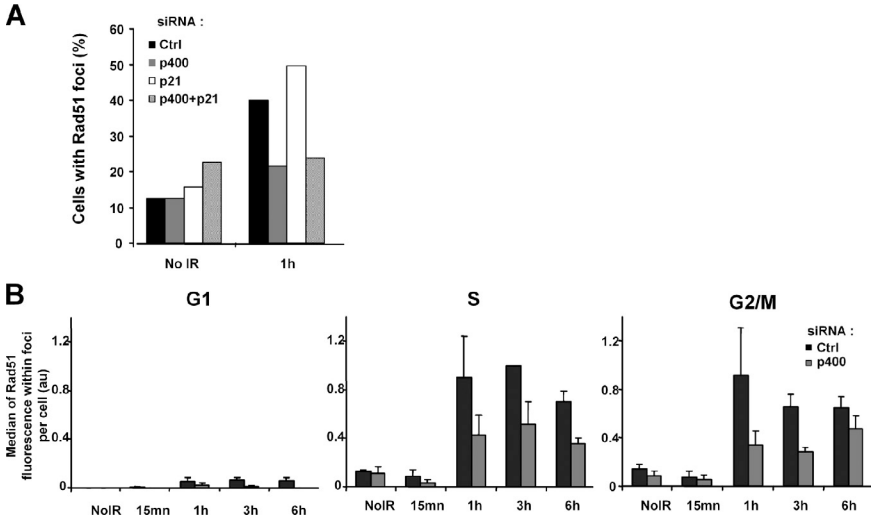

Figure 7. **The effect of p400 depletion on Rad51 foci formation is not caused by cell cycle changes.** (A) U2OS cells transfected with p400 and p21 siRNA alone or in combination were tested for Rad51 foci formation after IR as described in Fig. 6. The data shown are from a single representative experiment (100 cells/point) out of three repeats. (B) Medians of Rad51 levels within foci per cell for G1, S, and G2/M cell populations (analyzed using the Arrayscan) were calculated for U2OS cells transfected with control or p400 siRNA exposed to 8 Gy. Results were standardized relative to 1 for the highest median (3 h after irradiation for S phase cells transfected with control siRNA). The means and SD from four independent experiments are plotted.

the effect of DNA damage induction on the ability of p400 and Rad51 to interact. By coimmunoprecipitation from RG37 cells extracts, we observed that p400 and Rad51 still interact after IR (Fig. 8 D). We also performed FRET-based experiments in U2OS cells stably expressing ER-AsiSI in which OHTam treatment induces DSB (Fig. S4 D; Iacovoni et al., 2010). We found that FRET efficiency is unchanged upon DSB induction (Fig. 8 E). Thus, collectively, these results indicate that p400 and Rad51 are present in the same complex before and after DSB.

p400 and Rad51 work together to promote histone removal associated with HR

We next investigated the role of the p400–Rad51 complex in HR. Because p400 is an ATP-dependent chromatin remodeling enzyme (Kusch et al., 2004; Mizuguchi et al., 2004), we tested whether p400 participates in HR by affecting chromatin remodeling. We first used a mutant form of p400 devoid of ATPase activity (p400dead; Samuelson et al., 2005). This mutant interacts as efficiently with Rad51 as the wild type (Fig. S5 B) and is

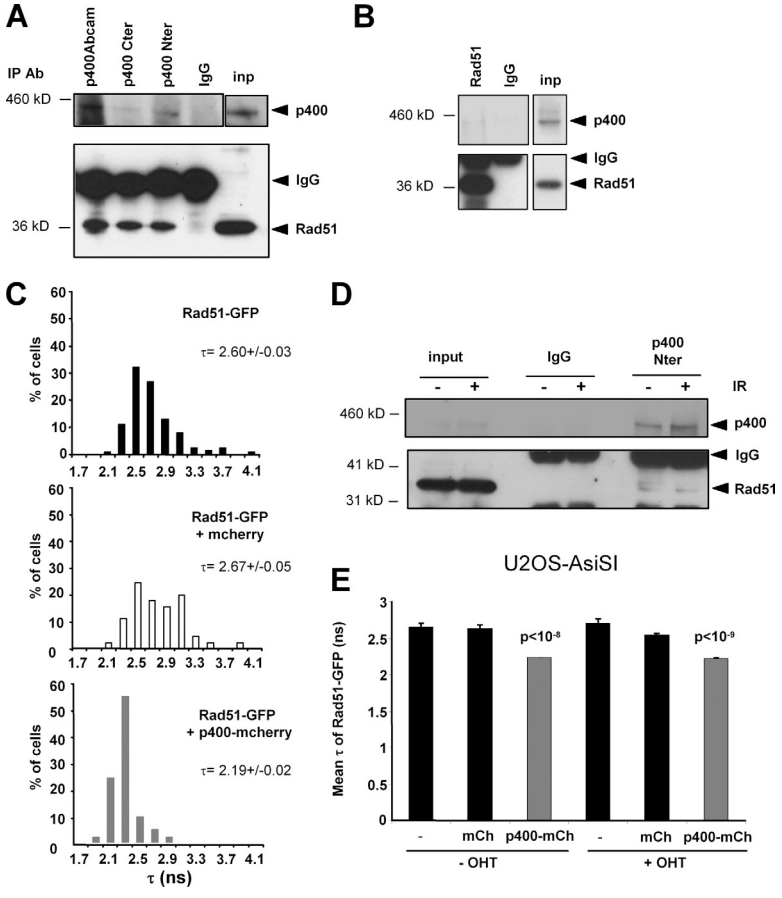

Figure 8. **p400 interacts with Rad51.** (A) RG37 total cell extracts were immunoprecipitated with three different p400 antibodies or control IgG and the presence of Rad51 was analyzed by Western blotting. (B) HeLa nuclear extracts were immunoprecipitated by Rad51 or control IgG as indicated. Immunoprecipitates were subjected to an elution step with 0.1% SDS. Eluted proteins or beads were subjected to a p400 or Rad51 Western blot, respectively. (C) RG37 cells were transfected with Rad51-GFP alone (n = 115) or together with vectors expressing p400-mcherry (n = 101) or mcherry (n = 45), as indicated. 24 h later, GFP fluorescence lifetime values were measured on representative cells. (D) RG37 total cell extracts were immunoprecipitated with p400 antibody or control IgG 3 h after 8 Gy exposure and the presence of Rad51 was analyzed by Western blotting. (E) Mean value and SEM of GFP fluorescence lifetime in U2OS-AsiSI cells without DSB induction (−OHT) and after DSB induction (+OHT). The results were obtained from two independent experiments.

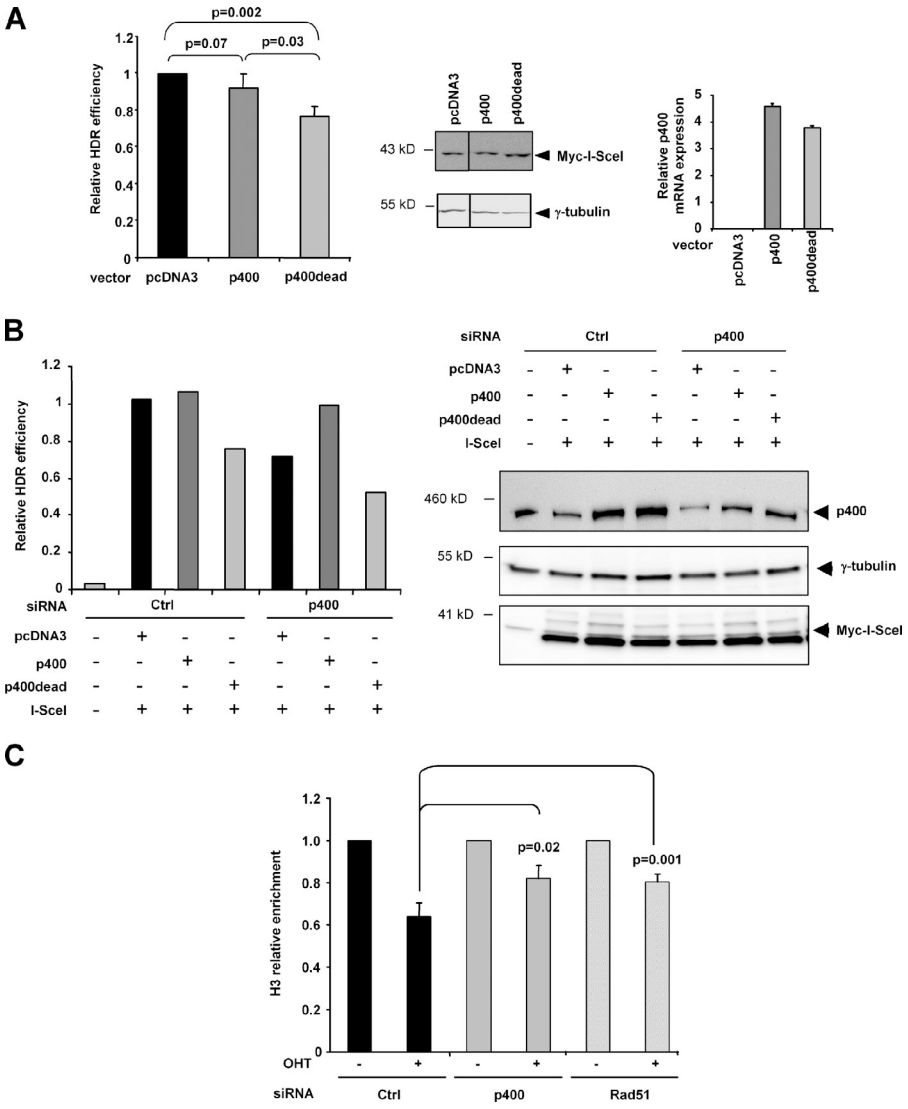

Figure 9. **Effects of p400-inactive form and complementation of the effects of p400 depletion on HR.** (A) RG37 cells were transfected with I-SceI expression vector (1 µg) together with p400 or p400dead (0.5 µg) as indicated. 48 h later, HDR efficiency was measured by FACS. The mean ± SD from three independent experiments is shown (left). Western blot monitoring the expression of myc-I-SceI and an RT-PCR analysis monitoring the expression of exogenous p400 and p400dead mRNA are also shown (right). (B) RG37 cells were transfected with the indicated siRNA. 24 h later, they were transfected by vectors expressing p400 or p400dead (0.5 µg) and I-SceI (1 µg) as indicated. 48 h later, HDR efficiency was measured by FACS. The data shown are from a single representative experiment (n = 25,000 events) out of three repeats (left). A Western blot monitoring p400 and myc-I-SceI expression is shown. (C) AsiSI-ER-U2OS cells were transfected with control, p400, or Rad51 siRNAs, and 48 h later treated with OHTam for 4 h. Cells were then subjected to ChIP analysis using H3 antibodies. The amount of a sequence located at 200 bp from a cleaved Asi-S1 site was quantified by qPCR. Results were standardized relative to the ChIP efficiency on a control sequence (P0) and expressed relative to 1 in untreated cells. Data are the mean ± SD from five independent experiments.

likely to function as a dominant-negative mutant for the chromatin remodeling activity of the p400–Rad51 complex. We cotransfected RG37 cells with I-SceI and p400 or p400dead plasmids and examined HDR. HDR efficiency is decreased in cells transfected with p400dead (Fig. 9 A), showing the importance of p400 enzymatic activity. Because this effect is modest, we intended to complement the effects of p400 siRNA by reexpressing p400 from plasmid constructs. We used the p400-2 siRNA, which is directed against the 5′ untranslated region that is absent in the p400 wild-type or mutant expression vectors. We transfected RG37 cells with siRNAs and 24 h later we transfected these cells again with expression vectors for p400, p400dead, or empty vector together with the I-SceI expression vector. Strikingly, whereas the wild type p400 is able to complement the effect of the siRNA, the p400dead mutant further decreases HDR efficiency (Fig. 9 B). Because the expression of p400 wild type and dead mutant are comparable, this result confirms that the ATPase activity of p400 is required for HDR. We next investigated whether p400 participates in the chromatin remodeling associated with HR. Indeed, nucleosome occupancy decreases in the vicinity of a sequence-specific DNA break (Berkovich et al., 2007; Xu et al., 2010). Using the AsiSI-expressing cell line, we monitored nucleosome occupancy by performing histone H3 ChIP analysis. In control cells, DNA break induction leads to a decrease in histone H3 occupancy in the vicinity of the break at which Rad51 is recruited (Fig. 9 C). In cells transfected by p400 and Rad51 siRNAs, this decrease is much lower (Fig. 9 C). Thus, p400 and Rad51 are both required for the decrease of nucleosome occupancy around DNA breaks. Collectively, these results are consistent with the possibility that the p400–Rad51 complex participates in the local removal of nucleosomes associated with the HR process.

Discussion

Here, we performed a comprehensive analysis of p400 function in DNA damage signaling and repair after exogenous DNA damage induction. Our data first indicate that p400 probably functions as a repressor of DNA damage signaling. Indeed, we observe an increase in γH2AX presence within foci upon p400 depletion as early as 15 min after IR (Fig. 2 A). This increase was found to be independent of the cell cycle phase (unpublished

data) and is not caused by an increase in the amount of DSBs (Fig. 1 G). It is probably because of the role of p400 in controlling ATM phosphorylation because we found that p400 depletion favors ATM phosphorylation upon DSB induction. The mechanism by which p400 represses ATM activation is unclear. However, three (not exclusive) hypotheses can be put forward. First, p400 could control ATM phoshorylation directly. Second, it could regulate ATM activation by inhibiting Tip60. Indeed, Tip60 is known to facilitate ATM autophosphorylation and activation via direct acetylation (Sun et al., 2005), and p400 can function as a repressor of Tip60 histone acetyl transferase (Tyteca et al., 2006; Park et al., 2010). Moreover, we previously showed that ATM phosphorylation in response to oncogenic stress, which induces replication-dependent DSBs, is also inhibited by p400 in a Tip60-dependent fashion (Mattera et al., 2009). Third, through its action on chromatin structure, it could also prevent the propagation of γH2AX, therefore limiting the size of IRIF, as recently proposed (Brunton et al., 2011). Consistent with this hypothesis, domino, the p400 homologue in flies, can remove phosphorylated histone H2Av from chromatin (Kusch et al., 2004).

We next found that all steps of DNA damage signaling and repair up to the formation of BRCA1 and Rad51 foci are not defective upon p400 depletion. These results stand in contrast to a recent study (Xu et al., 2010), which suggested a role of p400 in the retention of DNA repair proteins on DSBs via the regulation of histone ubiquitination by RNF8/RNF168. Indeed, Xu et al. (2010) showed that p400 is required for the RNF8-dependent ubiquitination of chromatin adjacent to DSB as well as for 53BP1 foci formation. We do not observe any defects in RNF8-mediated ubiquitination using the same FK2 antibody nor in 53BP1 foci formation upon p400 knockdown (Fig. 4). Importantly, we obtained these results in two different cell types (U2OS and 293T cells) using two doses of irradiation (2 and 8 Gy) in extended kinetics and using both a siRNA- and dominant-negative–based strategy. We thus conclude that the defect in RNF8-mediated ubiquitination observed by Xu et al. (2010) is probably specific to very particular experimental conditions and cannot be generalized.

We also investigated what happens after the peak of DNA damage signaling. We observed that the decrease in γH2AX levels is slower upon p400 depletion. This could reflect a role of p400 in removing γH2AX from chromatin after the completion of DNA repair, as described for the *D. melanogaster* homologue of p400 (Kusch et al., 2004). However, such a mechanism cannot entirely explain our findings that the effect of p400 on γH2AX foci disappearance is restricted to S and G2 phases of the cell cycle, a finding which is difficult to reconcile with a direct role of p400 in γH2AX removal. Moreover, using neutral comet assay to monitor detection of DSBs, we found that p400 depletion led to a defect in the removal of these breaks, demonstrating that DSB repair is deficient. Finally, the effects of p400 depletion are phenocopied by the depletion of a DNA repair protein, Rad51. Thus, the defective decrease of γH2AX after the peak of γH2AX foci formation in p400-depleted cells is caused, at least in part, by the presence of unrepaired DNA breaks that sustain DNA damage signaling.

Our data clearly indicate that p400 is particularly important for HR. This is indicated by several lines of evidence: (a) the defect in γH2AX removing after the peak of γH2AX foci formation upon p400 depletion is restricted to S and G2/M cells, as expected for a defect in HR; (b) p400 depletion leads to defective HDR; and (c) p400 depletion affects the formation of Rad51 and BRCA1 foci, two actors of HR.

Interestingly, DNA resection, at least monitored by phospho-RPA presence, seems to be normal in p400-depleted cells. This raises the question of the fate of DSBs that were subjected to a large resection. Indeed, such breaks should no longer be repaired by NHEJ because the extent of resection is proposed to mediate the choice between NHEJ and HR (Symington and Gautier, 2011). Our data on γH2AX foci numbers or using comet assays indicate that the number of breaks still declines, although more slowly, in the absence of p400. Thus, this result suggests that p400 depletion does not completely stop HR but only induces a delay. Consistent with such a possibility, we reproducibly found that Rad51 and BRCA1 foci eventually form 6 h after irradiation in p400-depleted cells (Fig. 6, C–H). Importantly, we found residual repair activity in MEFs in which the two alleles of p400 are mutated (Fig. S3). This last result suggests that the delayed HR observed upon p400 depletion is not caused by the residual p400 expression in siRNA-transfected cells but that p400 is not absolutely required for HR. Whether p400 absence can eventually be complemented by another ATPase is a possibility worth investigating.

What is the mechanism by which p400 participates in HR? As p400 can influence transcription, we examined results of DNA microarrays obtained after p400 depletion in U2OS cells (Mattera et al., 2010). We did not find any decrease in the expression of genes coding for DNA repair proteins involved in HR, and we confirmed this result by Western blot experiments for Rad51 (Fig. 3 D), Rad52, and BRCA1 (unpublished data; although in some experiments in U2OS cells we noticed a slight decrease in Rad51 and BRCA1 expression, perhaps reflecting a change in cell cycle distribution). Although we cannot rule out the possibility that p400 could affect the expression of another HR-linked protein, the reported p400 localization at the DSB site (Xu et al., 2010) supports a direct role for p400 in HR. The demonstration of a physical interaction between p400 and Rad51 (Fig. 8) suggests that p400 can directly affect Rad51 function. Note, however, that the proportion of Rad51 in complex with p400 is very low before and after DNA breaks, suggesting that it is not the only factor explaining p400's role in HR. For example, p400 could assist BRCA1 recruitment to chromatin, which, in turn, would facilitate Rad51 foci formation, in agreement with the known function of BRCA1. Our results indicate that the role of p400 in HR is strongly linked to Rad51 because the effects of p400 knockdown are very similar to the effects of Rad51 knockdown, with respect to nucleosome destabilization around the break (Fig. 9 C), HDR deficiency (Fig. 3), and maintenance of γH2AX foci (Fig. 2). These data together with the demonstration of the p400–Rad51 physical interaction suggest that p400 functions in HR at Rad51-dependent steps. Other ATP-dependent chromatin remodeling enzymes have been shown to be important for DNA damage response

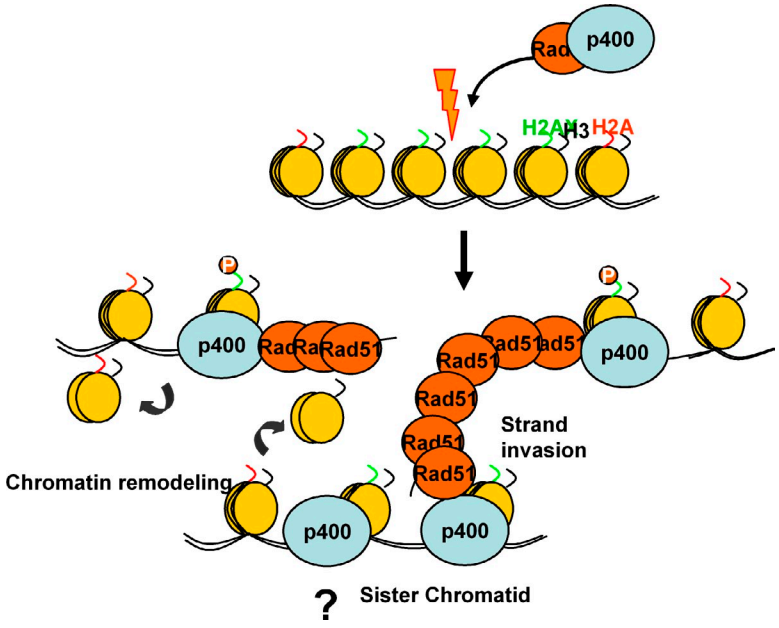

Figure 10. **Chromatin remodeling around Rad51-targeted DSB is dependent on p400 and Rad51.** Model for the coordinated action of p400 and Rad51 for the repair of DSB by HR. The p400–Rad51 preformed complex is recruited on chromatin after DSB, where it participates in the chromatin remodeling associated with HR. We speculate that this chromatin remodeling could occur on the cut DNA and/or on the uncut sister chromatid to favor strand invasion.

in mammals. However, most of these proteins function at earlier steps of DNA damage processing, such as histone ubiquitination; for example, CHD4 is required for histone ubiquitination after DSB (Larsen et al., 2010; Smeenk et al., 2010). To our knowledge, the only ATP-dependent chromatin remodeling protein known to function with Rad51 is Rad54, raising the important question of the relationship between p400 and Rad54. Importantly, the role of p400 seems to be very similar to that described for Rad54 because Rad54 can interact with Rad51 (Golub et al., 1997) and favors Rad51 recruitment to chromatin (Agarwal et al., 2011). Whether they function together on the same DSB or on different DSBs depending on chromatin state remains to be investigated.

The demonstration of the existence of a preformed p400–Rad51 complex important for HR indeed suggests a model in which both proteins need to be mobilized together after DSB (Fig. 10). This complex is likely to be rapidly mobilized in the vicinity of DSB because both Rad51 and p400 are recruited to DSB (Murr et al., 2006; Rodrigue et al., 2006; Xu et al., 2010). Moreover, consistent with this model, the yeast homologue of p400 (SWR1) is recruited very early to DNA breaks (van Attikum et al., 2007). Because of the role of Rad51 in strand invasion, one can speculate that the p400–Rad51 complex is involved in chromatin remodeling on the uncut strand to allow strand invasion (Fig. 10). Importantly, SWR1 is not required for HR (van Attikum et al., 2007), probably because of differences in chromatin states between yeast and humans. However, a link between Rad51 and p400 functions is conserved throughout evolution since when strand invasion is made defective in *S. cerevisiae* because of the absence of homologous sequences, SWR1 (the *S. cerevisiae* homologue of p400) and Rad51 functionally cooperate to target these DNA breaks to the nuclear periphery (Kalocsay et al., 2009). Clearly, understanding the bases of the coordination between DNA repair, chromatin remodeling, and nuclear positioning is a major challenge in the field.

Materials and methods

Antibodies, plasmids, and siRNAs

The commercial p400 antibody was purchased from Abcam, the Rad51 antibodies from Santa Cruz Biotechnology, Inc. (Rad51-H92; for ChIPs and some Western blot experiments) or from EMD Millipore (for some Western blot experiments), the p21 antibody (C19) from Santa Cruz Biotechnology, Inc., the HA antibody from Covance (HA-11), the myc antibody from Roche (9E10), the γH2AX antibodies from EMD Millipore for immunofluorescence experiments (JBW301) and from Epitomics for Western blot experiments, the actin and γ-tubulin antibodies from Sigma-Aldrich (T6199), the phospho-ATM antibody from Cell Signaling technology (10H11.E12), the lamin A/C antibody from Tebu-Bio (636), the phospho-RPA antibodies from Bethyl Laboratories, Inc. (S4-8) for immunofluorescence and (S33) for Western blot experiments, p-ChK2 antibody from Cell Signaling Technology (T68), BRCA1 antibody from Santa Cruz Biotechnology, Inc. (D-9), the FK2 antibody from EMD Millipore, the Rad52 antibody from Abcam, and the 53BP1 antibody from Novus Biologicals. Secondary antibodies were purchased from GE Healthcare and Sigma-Aldrich. Two other antibodies directed against p400 were raised by immunization of rabbits with peptide directed against the N- (RERRPSQPHTQSGGT) or C-terminal (PREEGKSKNNRPLRTSQC) sequence of the protein (Millegen).

pcDNA3βmycNLS-I-SceI plasmid and the corresponding empty plasmid were used. pcDNA3B-CMV-Flag-p400 plasmid was a gift from D. Livingston (Harvard University, Boston, MA). pCDNA3B-CMV-Flag-p400dead was constructed with the quick change site-directed mutagenesis kit (Agilent Technologies) according to the manufacturer's conditions to generate the K1085L mutation (Samuelson et al., 2005). For pEGFP-Rad51, Rad51 cDNA was cloned in the pEGFP-C1 plasmid (inserted into SalI–BamHI sites) and was a gift of A. Venkitaraman (University of Cambridge, Cambridge, UK). Construction of the pBabe-I-SceI-ER expression vector was performed by PCR amplification of the I-SceI sequence using primers to generate BglII–SalI sites. The PCR fragments were digested and inserted into BamHI–SalI sites of the pBabe vector in fusion with the HA-tagged ligand-binding domain of the estrogen receptor.

All siRNAs were purchased from Eurogentec. The control siRNA does not recognize any human mRNA. The efficiency of siRNA silencing was checked in each experiment by reverse transcription followed by real-time PCR or Western blot analysis.

The sequences of the top strands of the various siRNAs were as follow: Si control, CAUGUCAUGUGUCACAUCU-dTdT; Si p400, UGAAGAAGGUUCCCAAGAA-dTdT; Si p400-2, CGACACAUUGGAUACAGAA-dTdT; Si p21, GACCAUGUGGACCUGUCAC-dTdT; Si Rad51, CCAGAUCUGUCAUACGCUA-dTdT.

The following primer pairs were used to amplify cDNAs after reverse transcription experiments: p400, 5′-CTGCTGCGAAGAAGCTCGTT-3′

and 5′-CAATTCTTTCCCTCTCCTGC-3′; GAPDH, 5′-GAAGGTGAAGGTCGGAGTCA-3′ and 5′-GAAGATGGTGATGGGATTTC-3′; P0, 5′-GGCGACCTGGAAGTCCAACT-3′ and 5′-CCATCAGCACCACAGCCTTC-3′; p400Flag, 5′-CGCCACCATGGACTACAAGGACGAC-3′ and 5′-TGCTCCTCACCCTCGCTGCCA-3′.

The following primer pairs were used to amplify sequences after ChIP experiments: P0, 5′-GGCGACCTGGAAGTCCAACT-3′ and 5′-CCATCAGCACCACAGCCTTC-3′; AsiSI site, 5′-GATTGGCTATGGGTGTGGAC-3′ and 5′-CATCCTTGCAAACCAGTCCT-3′.

Cell culture and transfections

The osteaosarcoma cell line U2OS and the human embryonic kidney cell line 293T were purchased from the American Type Culture Collection. The RG37 cell line has been derived from SV40-transformed GM639 human fibroblasts (Dumay et al., 2006). GCS5 cell line was derived from RG37 cells. Both cell lines were gifts from B. Lopez (Institut Gustave Roussy, Villejuif, France). $p400^{\Delta N/\Delta N}$ and $p400^{+/+}$ MEF cells have been derived from $mDom^{\Delta N/\Delta N}$ or $mDom^{+/+}$ mice (Ueda et al., 2007; a gift from R. Fukunaga, Osaka University, Osaka, Japan). U2OS, RG37, GCS5, HEK 293T, and MEF cells were grown at 37°C in DMEM supplemented with antibiotics and 10% FCS (all from Invitrogen). The AsiSI-ER-U2OS and U2OS-ER-ISceI stable cell lines were maintained in DMEM supplemented with antibiotics and 10% FCS. When needed, 300 nM of 4-OHTam was added to culture medium for 4 h. Stable transfectants from the pBabe HA-I-SceI-ER plasmid were obtained after hygromycin selection (500 µg/ml).

For siRNA transfection, 10^5 cells were transfected using Interferin (Ozyme) and 10 nM of siRNA according to the manufacturer's instructions. For all other experiments, 5×10^6 cells were transfected by electroporation using an Amaxa device with siRNAs (10 µM), according to the manufacturer's specifications. Plasmids were transfected with Jet-PEI (Ozyme) according to the manufacturer's instructions.

RNA extraction and reverse transcription

Total RNA was prepared with RNeasy mini kit (QIAGEN) and resuspended in 30 µl of RNase-free water. 1 or 2 µg of total RNA was reverse transcribed (50 min at 42°C) in buffer containing oligo-dT or random primers (0.5 µg), AMV RT buffer, 10 U of AMV reverse transcription, 40 U of rRNasin (Promega), 0.5 mM deoxynucleotides (Promega), and 10 mM DTT. The reactions were performed at 70°C (15 min) and then stopped. The cDNAs obtained were analyzed by q-PCR.

ChIP experiments

Cells were fixed in 1% formaldehyde (20 min) and glycine added to block the reaction. ChIPs were performed as described previously (Mattera et al., 2010) using 50 µg of chromatin (for histone H3 ChIP) or 200 µg of chromatin (for Rad51 ChIPs). In brief, nuclei were prepared and sonicated to generate DNA fragments with lengths between 500 and 1,000 bp. After preclearing and blocking steps, immunoprecipitations were performed overnight (4°C) with specific antibodies or without antibody as negative control. Recovering of the immune complexes was performed by the incubation of the samples with a mixture of blocked protein A/protein G beads on a rotating wheel (2 h at 4°C). After extensive washing, the DNA–protein cross-link was reversed by the addition of RNase A to the samples and heating at 65°C. After proteinase K digestion (1.5 h), DNA was purified using a spin column (GFX PCR kit; GE Healthcare), and then quantitated by qPCR using a DNA Engine Real-Time PCR machine (Bio-Rad Laboratories) according to the manufacturer's instructions. qPCR reactions were performed in triplicate.

Immunofluorescence and manual quantification

Cells on coverslips were fixed with formaldehyde (3.7% in PBS) for 15 min at RT, permeabilized in 0.5% Triton X-100 for 5 min, and blocked with 3% BSA for 30 min. Primary antibodies were diluted in PBS-BSA 0.5% and incubated for 1 h. Cells were washed three times with PBS and incubated 1 h with secondary antibody (conjugated to either Alexa Fluor 488, Alexa Fluor 594, or Alexa Fluor 647; Invitrogen). Image capture was performed at RT on slides mounted with Vectashield (Vector Laboratories). Images were collected with a microscope (DM5000; Leica) equipped with a charge-coupled device camera (CoolSNAP ES; Roper Scientific) and a 40× objective (HCX PL APO ON, NA 0.85) and SEMROCK filters. Acquisition software and image processing used the MetaMorph software package (Molecular Devices).

Quantification of fluorescence levels was done on ∼100–200 cells per slide using home-developed macros in ImageJ software (National Institutes of Health) to normalize background, thresholds, and measures, except FK2 and 53BP1 foci, which were quantified manually (cells with more than five foci were considered positive).

For all the immunofluorescences performed with Arrayscan analysis, U2OS and HEK 293T were plated in 96-well plates. For 293T, plates were coated with poly-L-lysin (Sigma-Aldrich). U2OS cells were treated to 0.5% Triton X-100 (2 min at 4°C) before the fixation with formaldehyde. Immunofluorescence was then performed as described in the previous paragraph.

Arrayscan analysis

The acquisition of images was obtained on an ArrayScan HCS reader with a 20× objective lens and effective image analyses were done by Cellomics Technologies (Compartmental Analysis version 4 Bioapplication; Thermo Fisher Scientific). The method was based on the spot detection before and after IR; parameters were chosen for each antibody to optimize the difference between untreated and irradiated cells. At the end of the acquisition analysis, we obtained raw data files for each sample as excel files indicating, for each cell, the size of the nucleus, the total amount of Hoechst fluorescence per nucleus, the total amount of relevant antibody fluorescence per nucleus, the number of foci, and the total amount of fluorescence within foci. We show in figures the medians for the cell population (∼200 cells per sample) of foci numbers or of total amount of fluorescence within foci because the median is more accurate than the mean when analyzing automatically obtained data (the mean can be strongly influenced by few artifactual high data). The statistical significance of the differences in the number of foci or in the total amount of fluorescence within foci between the control and p400 siRNA populations was analyzed using Student's *t* test assuming unequal variances. Note that for unknown reasons, the Arrayscan failed to analyze some Rad51 samples; they were thus omitted from the analysis (such as the 15-min point in Fig. 6 C and the 30-min and 1-h points in Fig. 6 D). Moreover, some points not essential to our conclusions and that were obviously aberrant and not reproducible were also removed from the figures (such as the 15-min point in Fig. 1 F).

Immunoprecipitations

Nuclear Extracts (100 µg) were diluted in buffer A supplemented with DNase (150 mM NaCl, 5 mM $MgCl_2$, 50 mM Tris, pH 8.0, 0.4% NP-40, 3 mM $CaCl_2$, and 0.75 U/ml DNase) and precleared with protein A beads (1 h at 4°C) on a rotating wheel. Immunoprecipitations were performed by adding 2 µg of antibodies to precleared extracts. After an overnight incubation at 4°C, 20 µl of a mixture of protein A/protein G beads were added for 1 h at 4°C. Beads were washed three times with supplemented buffer A and subjected to Western blotting. For Rad51 IP, an elution step was included: beads were incubated 10 min at room temperature with 30 µl of elution buffer (150 mM NaCl, 0.1% SDS, 5 mM MgCl2, 50 mM Tris, pH 8.0, and 0.4% NP-40). Beads and supernatant were subjected to a Western blot analysis for Rad51 and p400, respectively.

Western blot analysis

Total cell extracts were prepared by resuspending pelleted cells in Laemmli buffer (60 mM TrisHCl, pH 6.8, 10% glycerol, 2% SDS, 5% β-mercaptoethanol, and bromophenol blue; Chailleux et al., 2010). Preparation of nuclear extracts was performed as previously described (Tyteca et al., 2006; Mattera et al., 2009, 2010). In brief, trypsinized cells were resuspended in lysis buffer (10 mM NaCl, 2 mM $MgCl_2$, 10 mM TrisHCl, pH 8.0, and protease inhibitors) and incubated on ice (5 min), and then NP-40 was added for an additional 5 min. After centrifugation (2,000 *g* for 5 min), the pellet was resuspended in buffer (420 mM NaCl, 1.5 mM $MgCl_2$, 20 mM Hepes, pH 7.9, and 0.2 mM EDTA) for 30 min at 4°C on a rotating wheel. Samples were centrifuged at 20,000 *g* for 10 min and supernatants were collected. Equal amounts (10–25 µg) of proteins were loaded on NuPAGE Novex 4–12% Bis-tris gel or NuPAGE Novex 3–8% Tris-Acetate (Invitrogen) and transferred to nitrocellulose membrane. Membranes were blocked with 5% nonfat dry milk, incubated with primary antibodies for 1 h followed by peroxidase-conjugated secondary antibodies. Peroxidase activity was detected by using the Lumi-LightPLUS Western blotting substrate (Roche).

Neutral comet assay

Cells were harvested (∼10^4 per pellet), mixed with 100 µl low-melting-point agarose (0.7%) and layered onto agarose-coated glass slides. Slides were maintained in the dark at 4°C to gel until electrophoresis. Slides were submerged in lysis buffer (2.5 M NaCl, 0.1 M EDTA, 10 mM Trizma base, 1% N-laurylsarcosine, 0.5% Triton X-100, and 10% DMSO, pH 10) for 1 h. After lysis the slides were washed three times with the electrophoresis buffer (300 mM sodium acetate and 100 mM Tris-HCl, pH 8.3) and left in a fresh portion of the buffer for 1 h. After electrophoresis (1 h, 18 V), slides were fixed with EtOH and then stained with ethidium bromide (20 µg ml^{-1}).

Comet Tail Moment was scored for 100 cells/slide by using the Komet 6.0 (Andor Technology) software.

Assay for HDR

U2OS-ER-ISceI or RG37 cells were washed with PBS and treated with trypsin. Cells were resuspended in PBS and GFP-positive cells were analyzed by flow cytometry (FACScalibur; BD) to measure HDR. Quantification was performed on 2–5 x10^4 sorted events.

NHEJ assay

Transfection of GCS5 cells was performed with 10 nM siRNAs, and 48 h later with the I-SceI plasmid. After an additional 48 h, cells were resuspended in PBS and NHEJ events were scored by the quantification of GFP-positive cells by flow cytometry (FACScalibur). Quantification was performed on 2 × 10^4 sorted events.

FRET/FLIM

For FRET experiments the light source used was a modelocked Ti:sapphire laser (Tsunami 3941; Spectra-Physics). It was pumped by a 10-W diode laser (Millennia Pro; Spectra-Physics) and delivered ultrafast femtosecond pulses of light with 80 MHz frequency. Mean fluorescence decay profiles were calculated for each image for the entire nucleus. These data allowed the estimation of lifetimes by fitting these results with a mono-exponential function using a nonlinear least squares estimation procedure with the profile fitting function of the FLIM analysis software (Hamamatsu Photonics).

Statistics

Experimental differences were tested for significance using Student's *t* test for two samples, assuming unequal variances. Unless indicated otherwise, results represent the mean with error bars showing the SD.

Online supplemental material

Fig. S1 shows the efficiency of the silencing of p400, rad51, p21, and ATM in the different cell lines used in the various conditions and the effect of p400 depletion on cell cycle in U2OS and 293T cells. Fig. S2 shows that p400 depletion induces increased γH2AX staining in p400-deficient MEFs but does not affect 53BP1 foci formation. It also demonstrates that overexpression of p400 and p400dead does not affect the generation of 53BP1 and FK2 foci in 293T cells after IR. Fig. S3 shows the DSB repair activity using neutral comet assay in p400-defective MEFs exposed to IR. Fig. S4 shows the efficiency of the ER-I-SceI system in U2OS cells to induce DSBs as well as the cleavage efficiency on the cutting site examined for ChIP experiments. It also demonstrates the cleavage efficiency of the I-SceI site in RG37 cells after p400 depletion. Fig. S5 shows the interaction between rad51 and p400 in U2OS and RG37 cells. As positive control it also shows the interaction of Tip60 with p400. Online supplemental material is available online at http://www.jcb.org/cgi/content/full/jcb.201205059/DC1.

We thank R. Fukunaga and B. Lopez for materials, M. Quaranta for her help with flow cytometry, C. Briere for the statistical analysis of the FRET/FLIM data, F. Escaffit for his help in generating figures, and M. Chevillard-Briet for constructing the p400-mcherry construct. We are also grateful to P. Caron, G. Legube, B. Lopez, P. Bertrand, and all of D. Trouche's group members for helpful discussions. We acknowledge the use of the Toulouse Rio Imaging facilities for FACS and immunofluorescence experiments.

This work was supported by grants from the Ligue Nationale Contre le Cancer (D. Trouche; équipe labellisée), the Association de Recherche contre le Cancer (ARC) as a Programme ARC, the Agence Nationale pour la Recherche (Projet 2011 blanc SVSE8 PinGs), and by an Electricité de France grant (Y. Canitrot). We thank the Automatic high throughput image analysis facilities (Arrayscan), Institut National de la Santé et de la Recherche Médicale UMR1037-Cancer Research Center of Toulouse, University of Toulouse (supported by grants from Région Midi-Pyrénées and l'Institut National du Cancer [programme libre 2005 and 2008]). S. Briois was the recipient of a Fondation pour la Recherche Médicale fellowship.

Submitted: 9 May 2012
Accepted: 21 November 2012

References

Agarwal, S., W.A. van Cappellen, A. Guénolé, B. Eppink, S.E. Linsen, E. Meijering, A. Houtsmuller, R. Kanaar, and J. Essers. 2011. ATP-dependent and independent functions of Rad54 in genome maintenance. *J. Cell Biol.* 192:735–750. http://dx.doi.org/10.1083/jcb.201011025

Ahel, D., Z. Horejsí, N. Wiechens, S.E. Polo, E. Garcia-Wilson, I. Ahel, H. Flynn, M. Skehel, S.C. West, S.P. Jackson, et al. 2009. Poly(ADP-ribose)-dependent regulation of DNA repair by the chromatin remodeling enzyme ALC1. *Science*. 325:1240–1243. http://dx.doi.org/10.1126/science.1177321

Baumann, P., F.E. Benson, and S.C. West. 1996. Human Rad51 protein promotes ATP-dependent homologous pairing and strand transfer reactions in vitro. *Cell*. 87:757–766. http://dx.doi.org/10.1016/S0092-8674(00)81394-X

Berkovich, E., R.J. Monnat Jr., and M.B. Kastan. 2007. Roles of ATM and NBS1 in chromatin structure modulation and DNA double-strand break repair. *Nat. Cell Biol.* 9:683–690. http://dx.doi.org/10.1038/ncb1599

Brunton, H., A.A. Goodarzi, A.T. Noon, A. Shrikhande, R.S. Hansen, P.A. Jeggo, and A. Shibata. 2011. Analysis of human syndromes with disordered chromatin reveals the impact of heterochromatin on the efficacy of ATM-dependent G2/M checkpoint arrest. *Mol. Cell. Biol.* 31:4022–4035. http://dx.doi.org/10.1128/MCB.05289-11

Chai, B., J. Huang, B.R. Cairns, and B.C. Laurent. 2005. Distinct roles for the RSC and Swi/Snf ATP-dependent chromatin remodelers in DNA double-strand break repair. *Genes Dev.* 19:1656–1661. http://dx.doi.org/10.1101/gad.1273105

Chailleux, C., S. Tyteca, C. Papin, F. Boudsocq, N. Puget, C. Courilleau, M. Grigoriev, Y. Canitrot, and D. Trouche. 2010. Physical interaction between the histone acetyl transferase Tip60 and the DNA double-strand breaks sensor MRN complex. *Biochem. J.* 426:365–371. http://dx.doi.org/10.1042/BJ20091329

Chou, D.M., B. Adamson, N.E. Dephoure, X. Tan, A.C. Nottke, K.E. Hurov, S.P. Gygi, M.P. Colaiácovo, and S.J. Elledge. 2010. A chromatin localization screen reveals poly (ADP ribose)-regulated recruitment of the repressive polycomb and NuRD complexes to sites of DNA damage. *Proc. Natl. Acad. Sci. USA*. 107:18475–18480. http://dx.doi.org/10.1073/pnas.1012946107

Clapier, C.R., and B.R. Cairns. 2009. The biology of chromatin remodeling complexes. *Annu. Rev. Biochem.* 78:273–304. http://dx.doi.org/10.1146/annurev.biochem.77.062706.153223

Downs, J.A., S. Allard, O. Jobin-Robitaille, A. Javaheri, A. Auger, N. Bouchard, S.J. Kron, S.P. Jackson, and J. Côté. 2004. Binding of chromatin-modifying activities to phosphorylated histone H2A at DNA damage sites. *Mol. Cell*. 16:979–990. http://dx.doi.org/10.1016/j.molcel.2004.12.003

Dumay, A., C. Laulier, P. Bertrand, Y. Saintigny, F. Lebrun, J.L. Vayssière, and B.S. Lopez. 2006. Bax and Bid, two proapoptotic Bcl-2 family members, inhibit homologous recombination, independently of apoptosis regulation. *Oncogene*. 25:3196–3205. http://dx.doi.org/10.1038/sj.onc.1209344

Fuchs, M., J. Gerber, R. Drapkin, S. Sif, T. Ikura, V. Ogryzko, W.S. Lane, Y. Nakatani, and D.M. Livingston. 2001. The p400 complex is an essential E1A transformation target. *Cell*. 106:297–307. http://dx.doi.org/10.1016/S0092-8674(01)00450-0

Gévry, N., H.M. Chan, L. Laflamme, D.M. Livingston, and L. Gaudreau. 2007. p21 transcription is regulated by differential localization of histone H2A.Z. *Genes Dev.* 21:1869–1881. http://dx.doi.org/10.1101/gad.1545707

Golub, E.I., O.V. Kovalenko, R.C. Gupta, D.C. Ward, and C.M. Radding. 1997. Interaction of human recombination proteins Rad51 and Rad54. *Nucleic Acids Res.* 25:4106–4110. http://dx.doi.org/10.1093/nar/25.20.4106

Gospodinov, A., T. Vaissiere, D.B. Krastev, G. Legube, B. Anachkova, and Z. Herceg. 2011. Mammalian Ino80 mediates double-strand break repair through its role in DNA end strand resection. *Mol. Cell. Biol.* 31:4735–4745. http://dx.doi.org/10.1128/MCB.06182-11

Gottschalk, A.J., G. Timinszky, S.E. Kong, J. Jin, Y. Cai, S.K. Swanson, M.P. Washburn, L. Florens, A.G. Ladurner, J.W. Conaway, and R.C. Conaway. 2009. Poly(ADP-ribosyl)ation directs recruitment and activation of an ATP-dependent chromatin remodeler. *Proc. Natl. Acad. Sci. USA*. 106:13770–13774. http://dx.doi.org/10.1073/pnas.0906920106

Haaf, T., E.I. Golub, G. Reddy, C.M. Radding, and D.C. Ward. 1995. Nuclear foci of mammalian Rad51 recombination protein in somatic cells after DNA damage and its localization in synaptonemal complexes. *Proc. Natl. Acad. Sci. USA*. 92:2298–2302. http://dx.doi.org/10.1073/pnas.92.6.2298

Hoeijmakers, J.H. 2001. Genome maintenance mechanisms for preventing cancer. *Nature*. 411:366–374. http://dx.doi.org/10.1038/35077232

Iacovoni, J.S., P. Caron, I. Lassadi, E. Nicolas, L. Massip, D. Trouche, and G. Legube. 2010. High-resolution profiling of gammaH2AX around DNA double strand breaks in the mammalian genome. *EMBO J.* 29:1446–1457. http://dx.doi.org/10.1038/emboj.2010.38

Ikura, T., V.V. Ogryzko, M. Grigoriev, R. Groisman, J. Wang, M. Horikoshi, R. Scully, J. Qin, and Y. Nakatani. 2000. Involvement of the TIP60 histone acetylase complex in DNA repair and apoptosis. *Cell*. 102:463–473. http://dx.doi.org/10.1016/S0092-8674(00)00051-9

Ikura, T., S. Tashiro, A. Kakino, H. Shima, N. Jacob, R. Amunugama, K. Yoder, S. Izumi, I. Kuraoka, K. Tanaka, et al. 2007. DNA damage-dependent acetylation and ubiquitination of H2AX enhances chromatin dynamics. *Mol. Cell. Biol.* 27:7028–7040. http://dx.doi.org/10.1128/MCB.00579-07

Kalocsay, M., N.J. Hiller, and S. Jentsch. 2009. Chromosome-wide Rad51 spreading and SUMO-H2A.Z-dependent chromosome fixation in response to a persistent DNA double-strand break. *Mol. Cell*. 33:335–343. http://dx.doi.org/10.1016/j.molcel.2009.01.016

Kruhlak, M.J., A. Celeste, G. Dellaire, O. Fernandez-Capetillo, W.G. Müller, J.G. McNally, D.P. Bazett-Jones, and A. Nussenzweig. 2006. Changes in chromatin structure and mobility in living cells at sites of DNA double-strand breaks. *J. Cell Biol.* 172:823–834. http://dx.doi.org/10.1083/jcb.200510015

Kusch, T., L. Florens, W.H. Macdonald, S.K. Swanson, R.L. Glaser, J.R. Yates III, S.M. Abmayr, M.P. Washburn, and J.L. Workman. 2004. Acetylation by Tip60 is required for selective histone variant exchange at DNA lesions. *Science*. 306:2084–2087. http://dx.doi.org/10.1126/science.1103455

Lan, L., A. Ui, S. Nakajima, K. Hatakeyama, M. Hoshi, R. Watanabe, S.M. Janicki, H. Ogiwara, T. Kohno, S. Kanno, and A. Yasui. 2010. The ACF1 complex is required for DNA double-strand break repair in human cells. *Mol. Cell*. 40:976–987. http://dx.doi.org/10.1016/j.molcel.2010.12.003

Larsen, D.H., C. Poinsignon, T. Gudjonsson, C. Dinant, M.R. Payne, F.J. Hari, J.M. Rendtlew Danielsen, P. Menard, J.C. Sand, M. Stucki, et al. 2010. The chromatin-remodeling factor CHD4 coordinates signaling and repair after DNA damage. *J. Cell Biol.* 190:731–740. http://dx.doi.org/10.1083/jcb.200912135

Lee, H.S., J.H. Park, S.J. Kim, S.J. Kwon, and J. Kwon. 2010. A cooperative activation loop among SWI/SNF, gamma-H2AX and H3 acetylation for DNA double-strand break repair. *EMBO J.* 29:1434–1445. http://dx.doi.org/10.1038/emboj.2010.27

Llères, D., M. Denegri, M. Biggiogera, P. Ajuh, and A.I. Lamond. 2010. Direct interaction between hnRNP-M and CDC5L/PLRG1 proteins affects alternative splice site choice. *EMBO Rep.* 11:445–451. http://dx.doi.org/10.1038/embor.2010.64

Luijsterburg, M.S., and H. van Attikum. 2012. Close encounters of the RNF8th kind: when chromatin meets DNA repair. *Curr. Opin. Cell Biol.* 24:439–447. http://dx.doi.org/10.1016/j.ceb.2012.03.008

Mailand, N., S. Bekker-Jensen, H. Faustrup, F. Melander, J. Bartek, C. Lukas, and J. Lukas. 2007. RNF8 ubiquitylates histones at DNA double-strand breaks and promotes assembly of repair proteins. *Cell*. 131:887–900. http://dx.doi.org/10.1016/j.cell.2007.09.040

Mattera, L., F. Escaffit, M.J. Pillaire, J. Selves, S. Tyteca, J.S. Hoffmann, P.A. Gourraud, M. Chevillard-Briet, C. Cazaux, and D. Trouche. 2009. The p400/Tip60 ratio is critical for colorectal cancer cell proliferation through DNA damage response pathways. *Oncogene*. 28:1506–1517. http://dx.doi.org/10.1038/onc.2008.499

Mattera, L., C. Courilleau, G. Legube, T. Ueda, R. Fukunaga, M. Chevillard-Briet, Y. Canitrot, F. Escaffit, and D. Trouche. 2010. The E1A-associated p400 protein modulates cell fate decisions by the regulation of ROS homeostasis. *PLoS Genet.* 6:e1000983. http://dx.doi.org/10.1371/journal.pgen.1000983

Meyn, M.S. 1993. High spontaneous intrachromosomal recombination rates in ataxia-telangiectasia. *Science*. 260:1327–1330. http://dx.doi.org/10.1126/science.8493577

Mizuguchi, G., X. Shen, J. Landry, W.H. Wu, S. Sen, and C. Wu. 2004. ATP-driven exchange of histone H2AZ variant catalyzed by SWR1 chromatin remodeling complex. *Science*. 303:343–348. http://dx.doi.org/10.1126/science.1090701

Morrison, A.J., J. Highland, N.J. Krogan, A. Arbel-Eden, J.F. Greenblatt, J.E. Haber, and X. Shen. 2004. INO80 and gamma-H2AX interaction links ATP-dependent chromatin remodeling to DNA damage repair. *Cell*. 119:767–775. http://dx.doi.org/10.1016/j.cell.2004.11.037

Murr, R., J.I. Loizou, Y.G. Yang, C. Cuenin, H. Li, Z.Q. Wang, and Z. Herceg. 2006. Histone acetylation by Trrap-Tip60 modulates loading of repair proteins and repair of DNA double-strand breaks. *Nat. Cell Biol.* 8:91–99. http://dx.doi.org/10.1038/ncb1343

Neumaier, T., J. Swenson, C. Pham, A. Polyzos, A.T. Lo, P. Yang, J. Dyball, A. Asaithamby, D.J. Chen, M.J. Bissell, et al. 2012. Evidence for formation of DNA repair centers and dose-response nonlinearity in human cells. *Proc. Natl. Acad. Sci. USA*. 109:443–448. http://dx.doi.org/10.1073/pnas.1117849108

Nievergall, E., P.W. Janes, C. Stegmayer, M.E. Vail, F.G. Haj, S.W. Teng, B.G. Neel, P.I. Bastiaens, and M. Lackmann. 2010. PTP1B regulates Eph receptor function and trafficking. *J. Cell Biol.* 191:1189–1203. http://dx.doi.org/10.1083/jcb.201005035

Oum, J.H., C. Seong, Y. Kwon, J.H. Ji, A. Sid, S. Ramakrishnan, G. Ira, A. Malkova, P. Sung, S.E. Lee, and E.Y. Shim. 2011. RSC facilitates Rad59-dependent homologous recombination between sister chromatids by promoting cohesin loading at DNA double-strand breaks. *Mol. Cell. Biol.* 31:3924–3937. http://dx.doi.org/10.1128/MCB.01269-10

Papamichos-Chronakis, M., J.E. Krebs, and C.L. Peterson. 2006. Interplay between Ino80 and Swr1 chromatin remodeling enzymes regulates cell cycle checkpoint adaptation in response to DNA damage. *Genes Dev.* 20:2437–2449. http://dx.doi.org/10.1101/gad.1440206

Park, J.H., X.J. Sun, and R.G. Roeder. 2010. The SANT domain of p400 ATPase represses acetyltransferase activity and coactivator function of TIP60 in basal p21 gene expression. *Mol. Cell. Biol.* 30:2750–2761. http://dx.doi.org/10.1128/MCB.00804-09

Puget, N., M. Knowlton, and R. Scully. 2005. Molecular analysis of sister chromatid recombination in mammalian cells. *DNA Repair (Amst.)*. 4:149–161. http://dx.doi.org/10.1016/j.dnarep.2004.08.010

Rodrigue, A., M. Lafrance, M.C. Gauthier, D. McDonald, M. Hendzel, S.C. West, M. Jasin, and J.Y. Masson. 2006. Interplay between human DNA repair proteins at a unique double-strand break in vivo. *EMBO J.* 25:222–231. http://dx.doi.org/10.1038/sj.emboj.7600914

Rogakou, E.P., C. Boon, C. Redon, and W.M. Bonner. 1999. Megabase chromatin domains involved in DNA double-strand breaks in vivo. *J. Cell Biol.* 146:905–916. http://dx.doi.org/10.1083/jcb.146.5.905

Ruhf, M.L., A. Braun, O. Papoulas, J.W. Tamkun, N. Randsholt, and M. Meister. 2001. The domino gene of *Drosophila* encodes novel members of the SWI2/SNF2 family of DNA-dependent ATPases, which contribute to the silencing of homeotic genes. *Development*. 128:1429–1441.

Samuelson, A.V., M. Narita, H.M. Chan, J. Jin, E. de Stanchina, M.E. McCurrach, M. Narita, M. Fuchs, D.M. Livingston, and S.W. Lowe. 2005. p400 is required for E1A to promote apoptosis. *J. Biol. Chem.* 280:21915–21923. http://dx.doi.org/10.1074/jbc.M414564200

Smeenk, G., W.W. Wiegant, H. Vrolijk, A.P. Solari, A. Pastink, and H. van Attikum. 2010. The NuRD chromatin-remodeling complex regulates signaling and repair of DNA damage. *J. Cell Biol.* 190:741–749. http://dx.doi.org/10.1083/jcb.201001048

Sun, Y., X. Jiang, S. Chen, N. Fernandes, and B.D. Price. 2005. A role for the Tip60 histone acetyltransferase in the acetylation and activation of ATM. *Proc. Natl. Acad. Sci. USA*. 102:13182–13187. http://dx.doi.org/10.1073/pnas.0504211102

Symington, L.S., and J. Gautier. 2011. Double-strand break end resection and repair pathway choice. *Annu. Rev. Genet.* 45:247–271. http://dx.doi.org/10.1146/annurev-genet-110410-132435

Tsukuda, T., A.B. Fleming, J.A. Nickoloff, and M.A. Osley. 2005. Chromatin remodelling at a DNA double-strand break site in *Saccharomyces cerevisiae*. *Nature*. 438:379–383. http://dx.doi.org/10.1038/nature04148

Tyteca, S., M. Vandromme, G. Legube, M. Chevillard-Briet, and D. Trouche. 2006. Tip60 and p400 are both required for UV-induced apoptosis but play antagonistic roles in cell cycle progression. *EMBO J.* 25:1680–1689. http://dx.doi.org/10.1038/sj.emboj.7601066

Ueda, T., R. Watanabe-Fukunaga, H. Ogawa, H. Fukuyama, Y. Higashi, S. Nagata, and R. Fukunaga. 2007. Critical role of the p400/mDomino chromatin-remodeling ATPase in embryonic hematopoiesis. *Genes Cells*. 12:581–592. http://dx.doi.org/10.1111/j.1365-2443.2007.01080.x

van Attikum, H., O. Fritsch, B. Hohn, and S.M. Gasser. 2004. Recruitment of the INO80 complex by H2A phosphorylation links ATP-dependent chromatin remodeling with DNA double-strand break repair. *Cell*. 119:777–788. http://dx.doi.org/10.1016/j.cell.2004.11.033

van Attikum, H., O. Fritsch, and S.M. Gasser. 2007. Distinct roles for SWR1 and INO80 chromatin remodeling complexes at chromosomal double-strand breaks. *EMBO J.* 26:4113–4125. http://dx.doi.org/10.1038/sj.emboj.7601835

Xie, A., A. Kwok, and R. Scully. 2009. Role of mammalian Mre11 in classical and alternative nonhomologous end joining. *Nat. Struct. Mol. Biol.* 16:814–818. http://dx.doi.org/10.1038/nsmb.1640

Xu, Y., Y. Sun, X. Jiang, M.K. Ayrapetov, P. Moskwa, S. Yang, D.M. Weinstock, and B.D. Price. 2010. The p400 ATPase regulates nucleosome stability and chromatin ubiquitination during DNA repair. *J. Cell Biol.* 191:31–43. http://dx.doi.org/10.1083/jcb.201001160

Ziv, Y., D. Bielopolski, Y. Galanty, C. Lukas, Y. Taya, D.C. Schultz, J. Lukas, S. Bekker-Jensen, J. Bartek, and Y. Shiloh. 2006. Chromatin relaxation in response to DNA double-strand breaks is modulated by a novel ATM- and KAP-1 dependent pathway. *Nat. Cell Biol.* 8:870–876. http://dx.doi.org/10.1038/ncb1446